DOI:
10.1016/j.jhydrol.2019.04.064

Document Version
Peer reviewed version

Forests as 'sponges' and 'pumps': Assessing the impact of deforestation on dry-season flows across the tropics

Article *in* Journal of Hydrology · April 2019

DOI: 10.1016/j.jhydrol.2019.04.064

CITATIONS
0

READS
164

4 authors:

Jorge Peña-Arancibia
The Commonwealth Scientific and Industrial Research Organisation
34 PUBLICATIONS **661** CITATIONS
SEE PROFILE

L.A. Bruijnzeel
King's College London
202 PUBLICATIONS **8,533** CITATIONS
SEE PROFILE

Mark Mulligan
King's College London
115 PUBLICATIONS **2,908** CITATIONS
SEE PROFILE

Albert Ide Jan Martijn van Dijk
Australian National University
307 PUBLICATIONS **7,878** CITATIONS
SEE PROFILE

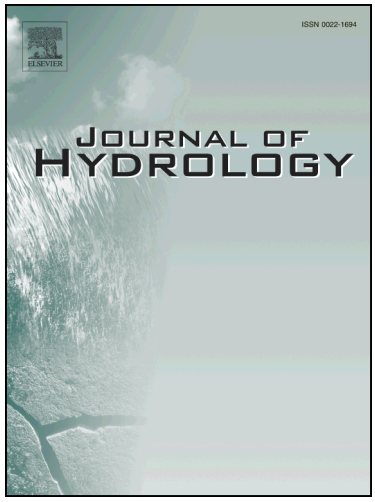

Research papers

Forests as 'sponges' and 'pumps': Assessing the impact of deforestation on dry-season flows across the tropics

Jorge L. Peña-Arancibia, L. Adrian Bruijnzeel, Mark Mulligan, Albert I.J.M. van Dijk

PII: S0022-1694(19)30403-2
DOI: https://doi.org/10.1016/j.jhydrol.2019.04.064
Reference: HYDROL 23701

To appear in: *Journal of Hydrology*

Received Date: 6 December 2018
Revised Date: 26 February 2019
Accepted Date: 18 April 2019

Please cite this article as: Peña-Arancibia, J.L., Bruijnzeel, L.A., Mulligan, M., I.J.M. van Dijk, A., Forests as 'sponges' and 'pumps': Assessing the impact of deforestation on dry-season flows across the tropics, *Journal of Hydrology* (2019), doi: https://doi.org/10.1016/j.jhydrol.2019.04.064

Forests as 'sponges' and 'pumps': Assessing the impact of deforestation on dry-season flows across the tropics

Jorge L. Peña-Arancibia[1,2] *, L. Adrian Bruijnzeel[2], Mark Mulligan[2], Albert I.J.M. van Dijk[3]

[1]*CSIRO Land and Water, GPO Box 1700, Canberra, 2601, ACT, Australia*

[2]*Department of Geography, King's College London, London WC2R 2LS, United Kingdom*

[3]*Fenner School of Environment & Society, ANU College of Science, Australian National University, Canberra, Australia*

*****Corresponding author

E-Mail: jorge.penaarancibia@csiro.au

CSIRO Land and Water

Black Mountain Science and Innovation Park

GPO Box 1700, Canberra ACT 2601 Australia

Tel.: +61-2- 6246 -5711; Fax: + 61-2-6246-5845.

For: JoH

Date: 15 February 2019

ABSTRACT

Forests act as 'pumps' through their evapotranspiration (E_{tot}) and as 'sponges' by enhancing soil infiltration capacity and moisture retention. Tropical deforestation and poor post-forest land management generally result in lower E_{tot}, but also reduce infiltration. Strongly diminished infiltration is typically accompanied by enhanced overland flow and can cause reduced groundwater recharge and baseflows. A grid-based land surface hydrological model (W3RA–LUM) was tailored to incorporate the trade-offs between the 'pump' and 'sponge' effects so to investigate where deforestation can be expected to have the greatest impacts on dry-season flows. Streamflow sensitivity analyses for scenarios with or without full forest cover and/or good versus poor surface infiltration were performed for: (i) selected tropical catchments with documented changes in streamflow after deforestation; and (ii) the tropics at large (23.5°N to 35°S, to include important seasonal montane forests). The catchment sensitivity analyses showed that W3A–LUM captured the streamflow response to imposed deforestation and changes in surface conditions reasonably well. For the tropics as a whole, an increase in mean annual streamflow of 18% was obtained for forest conversion (to pasture) only, versus 26% after an additional imposed reduction in surface infiltration. Much of the inferred flow increases concerned water-limited regions. A *reduction* in dry-season flows was predicted for nearly one-fifth of all grid cells (despite lower E_{tot} after forest conversion) after impaired infiltration, potential 'hot spots' of hydrological change after deforestation and reduced infiltration. The affected grid cells shared the following key characteristics: (i) strong seasonality; (ii) high infiltration capacity under forested conditions; (iii) sufficient wet-season precipitation to recharge deep soil- and groundwater stores; (iv) sufficient soil water storage under forested conditions to 'carry over' infiltrated wet-season rainfall into the subsequent dry season; and (v) slow groundwater recession maintaining baseflow throughout the dry season.

Our results demonstrate that forest removal in highly seasonal tropical catchments, whilst typically increasing mean annual water yield, can indeed decrease dry-season flows, depending on pre- and post-forest removal surface conditions and groundwater response times.

Key words: Hydrological modelling; infiltration; land-use change; low flows; Soil Conservation Service Curve Number method; streamflow regime.

1. Introduction

Agricultural expansion between 1980 and 2005 in the tropics (estimated at ~630 million ha; FAO, 2006) occurred mostly at the expense of forest (Gibbs et al., 2010). Around 20% of the global land surface area, most of it in the tropics, suffers from some form of land degradation associated with large-scale intensive post-forest land use (Bai et al., 2008; Gibbs and Salmon, 2015). Such land-use changes can greatly alter the hydrological response, at scales ranging from individual hillslopes (Chandler and Walter, 1998; Ghimire et al., 2013; Toohey et al., 2018) and headwater catchments (Brown et al., 2005; Liu et al., 2011; Krishnaswamy et al., 2012; Recha et al., 2012), to meso-scale catchments and large river basins (Madduma Bandara, 1997; Costa et al., 2003; Zhou et al., 2010; Liu et al., 2015; Van Noordwijk et al., 2017a,b) although effects tend to become less pronounced at larger scales (Rodriguez et al., 2010; Zhang et al., 2017). Deforestation impacts on annual and seasonal streamflow totals depend partly on the trade-off between the associated changes in evapotranspiration (the 'pump effect') and infiltration (the 'sponge effect') (Bruijnzeel, 2004). Typically, because forests exhibit both greater water uptake (transpiration) and higher interception losses compared to grasses and crops (Zhang et al., 2001; van Dijk et al., 2007), forest replacement by a (well-managed) shorter vegetation cover generally results in increases in annual streamflow, infiltration and groundwater recharge commensurate with the percentage of forest removed (Bruijnzeel, 1990; Brown et al., 2005; Zhou et al., 2015). Further, as long as surface infiltration characteristics are more or less maintained after forest conversion, the bulk of the annual streamflow increase occurs during conditions of baseflow (Bruijnzeel, 2004; Farley et al., 2005; Lyon et al., 2017). On the other hand, where productive activities (cropping, grazing, extractive tree plantations) have taken place for decades, the soils frequently show a marked decline in porosity, infiltrability, and water retention (Martinez and

Zinck, 2004; Ziegler et al., 2006; Mehta et al., 2008; Germer et al., 2009; Nyberg et al., 2012; Ghimire et al., 2014; Liu et al., 2015; Jiang et al., 2017; Zwartendijk et al., 2017). In seasonal tropical headwater catchments where soil disturbance and surface degradation have affected infiltration opportunities adversely, precipitation intensities typically exceed the surface infiltration capacity more frequently than previously under forested conditions, thereby promoting infiltration-excess overland flow (Chandler and Walter, 1998; Sandström, 1998; Bonell et al., 2010; Zimmermann et al., 2010; Ghimire et al., 2013) and enhanced peak discharges, sometimes to the point of negatively affecting the groundwater recharge that sustains streamflow during the dry season (Sandström, 1995; Roa-García et al., 2011; Recha et al., 2012; Krishnaswamy et al., 2013; Qazi et al., 2017), also at larger scales (> 1000 km^2; Madduma Bandara, 1997; Rodriguez et al., 2010; Liu et al., 2015; Lyon et al., 2017; Hou et al., 2018). Such findings raise important questions about the extent, magnitude and sensitivity of the (net) impacts of forest conversion on seasonal streamflow across the tropics. Also, any climatic effects on long-term trends in streamflow characteristics need to be separated from land-use effects for a proper evaluation (Beck et al., 2013; Liu et al., 2015; Lacombe et al., 2016; Lyon et al., 2017). Large-scale modelling studies of the impact of deforestation on streamflow behaviour have thus far focused mainly on the streamflow impacts induced by changes in evapotranspiration (Gordon et al., 2005; Mulligan and Burke, 2005; Trabucco et al., 2008; Mao and Cherkauer, 2009; Mishra et al., 2010; Zhang et al., 2017), whereas only a handful of studies have included the impact of changes in surface infiltration as well (Mahé et al., 2005; Liu et al., 2015; Lyon et al., 2017; cf. Zhou et al., 2015; Hou et al., 2018). Arguably, knowledge of changes in streamflow regimes after forest conversion assumes added importance in view of the projected increases in the world's tropical population and associated requirements of food, water and fibres (Alexandratos and Bruinsma, 2012).

In this study, an evaluated variant of the World Wide Water Resources Assessment model

(W3RA; van Dijk et al., 2013), was tailored to incorporate deforestation impacts on both the 'pump'- and 'sponge' effects (called the W3RA Land Use Model or W3RA–LUM), with the aim of assessing the impacts of deforestation and soil degradation on streamflow regimes across the tropics, emphasizing effects on dry-season flows. W3RA has been used in global and regional assessments to, among others, quantify evapotranspiration from irrigated areas (Van Dijk et al., 2018), forecasting dryland vegetation (Tian et al., 2019), estimating water storage depletion (Khaki et al., 2018) and develop satellite-based river gauging (Hou et al., 2018). Besides describing changes in land cover that directly affect evapotranspiration, the model's stormflow computational scheme is akin to the Soil Conservation Service Curve Number Method (USDA-SCS, 1985) which permits the modification of soil parameters that affect surface infiltration characteristics and therefore the production of storm runoff. Curve numbers were originally derived from recorded rainfall-runoff data for small (agricultural) catchments in the Mid-Western U.S.A. (Hawkins et al., 2009), hence care should be exercised in transferring values to other areas with possibly very different rainfall and soil characteristics like the tropics (cf. Ogden et al., 2017). Nevertheless, although empirical in their derivation, various studies have justified the curve-number equations on theoretical grounds (Schaake et al., 1996; Yu, 1998; Mishra and Singh, 2003) and through field measurements, also in the (sub-)tropics (Descheemaeker et al., 2008; Yu, 2012; Blair et al., 2014). Also, despite having been criticized for not representing (subsurface) runoff-generating processes in forest land explicitly (Ogden et al., 2017), the method has been used successfully to demonstrate changes in storm runoff associated with land-use change in very different environments (Descheemaker et al., 2008; Beck et al., 2009; El-Hames, 2012; Wang et al., 2012; Blair et al., 2014). More importantly, the SCS-CN approach is currently the only method amenable to global application that has a strong empirical basis and is responsive to changes in soil characteristics (cf. Hong and Adler, 2008; Zeng et al., 2017). The chief

objective of this paper is to assess where, and why, tropical deforestation can be expected to have the greatest impacts on dry-season flows. Two types of analysis, following a model evaluation, are conducted to achieve this: (i) a qualitative comparison of the simulated hydrological responses in W3RA-LUM against observed responses as a result of imposed changes in vegetation and/or soil condition for four catchments (3–175,360 km^2) in the seasonal tropics of Java, Tanzania, Amazonia and Sri Lanka that have well-documented hydrological changes after deforestation; and (ii) deforestation modelling scenarios across the tropics (23.5°N to 35°S, to include important seasonal montane forests) with and without concurrent changes in surface infiltration conditions, to obtain a more realistic assessment of 'real-world' deforestation impacts on water yield, and on dry-season flows in particular, finding 'hot spots' where deforestation has greater impact.

2. Methods and materials

2.1. Hydrological model structure

W3RA, on which W3RA–LUM is based, is a global implementation of the AWRA-L landscape hydrology model (Van Dijk, 2010a) that is used operationally by the Australian Bureau of Meteorology to produce national-scale water balance information (Frost et al., 2016). W3RA is a one-dimensional grid-based land surface model that uses lumped models of the water budget for the soil-, groundwater- and surface water stores as applied to individual grid cells. W3RA–LUM is run at a grid resolution of 1^o and at a daily time-step, commensurate with the resolution of high-quality long-term global climatic data-bases (see Section 2.2 below). A model evaluation of W3RA-LUM for 1432 tropical catchments with an area<10,000 km^2 (about the grid cell size of the model) and also for 12 large catchments with an area >10,000 km^2 is described in the Supplementary Material section. The structure of

W3RA, the equations describing the various hydrological processes it represents, and justifications for specific adopted parameter values are discussed by Van Dijk et al. (2013). The W3RA-component that partitions (net) precipitation into stormflow (overland flow) and infiltration, as well as the modules that simulate soil water- and groundwater flows are described in the Supplementary Material section. W3RA's stormflow module was modified in W3RA–LUM so as to allow incorporation of the effect of surface degradation on runoff generation (see below). The following hydrological processes are simulated by W3RA–LUM (Fig. 1): (i) partitioning of incident precipitation into interception evaporation and net precipitation; (ii) partitioning of net precipitation into infiltration, infiltration-excess overland flow, and saturation-overland flow; (iii) snow melt and snow accumulation (not used in the tropical variant used here); (iv) vertical water movement within a topsoil compartment, including infiltration, drainage and soil water evaporation; (v) vertical water movement within a shallow soil compartment including incoming (from the topsoil above) and exiting drainage (to the compartment below) as well as root water uptake (transpiration); (vi) vertical water movement within a deep soil compartment (same processes as distinguished for the shallow soil compartment); (vii) vertical water movement in a groundwater store including recharge, capillary rise and outflow; and (viii) surface water body dynamics, including inflows via overland flow and river discharge, losses via open-water evaporation, and catchment water accumulation (flooding) (cf. Van Dijk et al., 2013). In addition, vegetation cover is adjusted dynamically through a simple model that predicts water-related vegetation phenology (Van Dijk, 2010a). The version used here simplified any sub-grid variation in vegetation cover by considering only two 'hydrological response units' (HRUs): (a) deep-rooted, tall vegetation ('forest'), which can use water from the shallow and deep soil water stores; and (b) shallow-rooted short vegetation ('grassland), which can only use water from

the shallow- and top-soil water stores (Van Dijk, 2010a). Thus, soil-water and energy balances are simulated separately for each HRU.

<Figure 1 about here>

Regarding the equations describing stormflow production in W3RA and W3RA–LUM (see Equation S1 in the Supplementary Material), it can be shown (Van Dijk, 2010c) that the term describing infiltration-excess overland flow generation (i.e. the first term in Eq. S1) is mathematically equivalent to the stormflow term of the SCS-CN method (i.e., $Q_{CN,}$ mm d^{-1}):

$$Q_{CN} = \frac{\left(P_g - I_a\right)^2}{\left(P_g - I_a\right) + S_{\max}}, \tag{1}$$

where P_g is gross precipitation (mm), I_a is the initial abstraction loss (interception, initial infiltration losses and surface storage losses), and S_{max} is the (hypothetical) soil water storage capacity at which half of the net precipitation falling on an unsaturated soil is able to infiltrate while the other half runs off (USDA-SCS, 1985). To avoid the need for independent estimation of I_a, a linear relationship with S_{max} was proposed and empirically justified by Ponce and Hawkins (1996) as follows: $I_a = \lambda S_{max}$, where λ (the so-called initial abstraction ratio) was given a value of 0.2. Using the latter value in Eq. (1) yields:

$$Q_{CN} = \left(\frac{P_n}{P_n + S_{\max}}\right) P_n . \tag{2}$$

For convenience, S_{max} was related by Hawkins et al. (2009) to a dimensionless parameter whose value ranges between zero (for the maximum theoretical soil water storage S_{max}) and 100 (for a completely dry soil) and which is commonly referred to as the curve number (CN):

$$S_{\max} = \frac{25400}{CN} - 254 . \tag{3}$$

In the CN-approach, each catchment is assumed to be represented by a (dominant) 'Hydrological Soil Group' (HSG) and a 'Hydrological Soil Condition' (HSC). Four HSGs (groups A–D) are distinguished, which correspond to different classes of soil infiltration capacity: group A has 'high' infiltration capacities, while groups B, C and D have 'intermediate', 'low' and 'very low' infiltration capacities, respectively (USDA-SCS, 1985). Similarly, the effect of land cover and/or management is characterized by the HSC for which three categories ('good', 'fair' and 'poor') are distinguished. The hydrological soil condition is generally determined in the field considering such factors as vegetation density, fractional cover and thickness of surface litter, and surface roughness (USDA-SCS, 1985). Recent progress in remote sensing-based mapping of land use and land cover, and the availability of soil maps at a global scale have made the derivation of a global map of CN-values feasible, albeit within the limitations and uncertainties of the respective data sources (Hong and Adler, 2008; Zeng et al., 2017).

To tailor CN-values to tropical conditions, we first used the 1 km grid-cell Harmonised World Soil Database (FAO/IIASA/ISRIC/ISSCAS/JRC, 2012) – which is based on the FAO/UNESCO Soil Map of the World (FAO/UNESCO, 1977) – to derive a global map of HSGs in which the four drainage classes as distinguished by USDA-SCS (1985) were equated to the qualitative FAO drainage classification which is based on actual soil types (rather than texture only) and adjusted for tropical soil characteristics (Table 1).

<**Table 1 about here**>

Next, we compiled published CN-values for different HSGs, land-cover types and associated HSCs from USDA-SCS (1985) and Hong and Adler (2008). However, in contrast to Hong and Adler (2008) – who only considered 'fair' conditions when deriving their global CN-map – surface condition (i.e. HSC-class) was considered explicitly in the current effort

using a global satellite-based proxy of land degradation (Bai et al., 2008). Bai et al. (2008) used trends in the 15-day rain-use efficiency (RUE)-adjusted normalized difference vegetation index (NDVI) for 8 x 8 km grid cells between 1981 and 2003 to infer areas with a long-term decline in ecosystem functioning and productivity (in terms of NDVI) that were not related to precipitation effects. To derive a preliminary HSC-map for the tropics, an HSC-class was assigned to each grid cell of the Bai et al. (2008) global degradation map based on the slope (or lack thereof) of the negative RUE-adjusted normalised NDVI trend. 'Good' hydrological conditions were linked to grid cells showing a positive or no trend, 'fair' conditions to grid cells with trends between 0 and -0.02, and 'poor' conditions to trends smaller than -0.02. Subsequently, the 1 km grid-cell resolution UMD Global Land Cover Classification of Hansen et al. (2000) was used to characterise land use across the tropics. The 8 km x 8 km HSC-map was then subsampled to the 1 km grid-cell resolution of the land use/land cover- and HSG-maps. Finally, a pan-tropical map of CN-values was derived by linking the HSG- and HSC-maps to the corresponding CN-values listed in Table 2, which was subsequently re-sampled to the 1º grid-cell resolution used in W3RA–LUM by averaging the respective curve numbers of all land-cover types present within the grid cell.

<Table 2 about here>

2.2. Meteorological and biophysical input data

Gridded daily 1º resolution meteorological forcing data used in the present analysis included daily precipitation (P in mm), incoming short-wave radiation (SW_{down} in Wm^{-2}), and minimum and maximum temperatures (T_{min}, T_{max} in ºC) for 1948–2008 as taken from the 50-Year High-Resolution Global Dataset of Meteorological Forcings for Land Surface Modelling developed by Sheffield et al. (2006). These long-term time-series were used to

overcome any inter-annual and inter-decadal precipitation variability effects in the deforestation modelling scenarios.

The vegetation cover fractions for each HRU in W3RA–LUM were estimated from the 500 m resolution map of tree cover derived from MODIS reflectance data for the period 2000–2001 (Hansen et al., 2003). Each grid cell provided percentages of tall woody or grass vegetation, as well as bare ground and open water surfaces. Other biophysical data used in the energy balance computations (see Van Dijk (2010a) and Van Dijk et al. (2013) for details) included an albedo climatology (after Moody et al., 2005; http://modis-atmos.gsfc.nasa.gov/ALBEDO/), and wind speed (1983–1993; http://eosweb.larc.nasa.gov/sse/) to compute aerodynamic conductance for the estimation of plant transpiration.

2.3. Streamflow sensitivity analysis for selected tropical catchments

An initial streamflow sensitivity analysis was performed to qualitatively evaluate W3RA–LUM and the hydrological processes it simulates in response to changes in land-cover type and/or soil conditions for four comparatively data-rich tropical catchments (3–175,360 km^2) with documented changes in streamflow and representing seasonal conditions of varying intensity. The basic characteristics of these catchments and the types of land-cover and hydrological changes involved are listed in Table 3, whereas the corresponding observed long-term changes in streamflow regime for three out of the four catchments are shown in Fig. 2.

<Table 3 about here>

<Figure 2 about here>

Four different sensitivity simulations were conducted using W3RA–LUM for each of these four locations, viz. model runs with: (i) 100% forest cover (100FC); (ii) 0% forest cover (i.e., 100% grass cover, 0FC) without any change in soil condition; (iii) 100% forest cover with a maximum negative change in soil condition (100FCSC); and (iv) 0% forest cover and maximum negative change in soil condition (i.e., 0FCSC). These realisations would thereby impose upper and lower limits to test the trade-offs between the 'pump' and 'sponge' effects.

Runoff Curve Numbers for the 100FC-scenario were derived by supplanting grassland CN-values (Table 2) with those for the regionally dominant forest type (according to the UMD Global Land Cover Classification) and vice versa for the 0FC-scenario. It was also assumed that for the imposed negative change in soil condition SC, any decrease in forest cover was associated with a change from good to poor HSC (cf. Table 2), thus reflecting the most extreme case of soil disturbance, and vice versa for increases in forest cover. Subsequently, the simulations were conducted for each location and scenario using daily climatic data for the years 1948–2008 as input (Sheffield et al., 2006). The resulting plots of long-term mean monthly streamflow regimes were used to assess the robustness of the W3RA-LUM simulations by comparing them with the observed changes in flows (cf. Fig. 2).

2.4. Streamflow sensitivity analysis across the tropics

Streamflow sensitivity simulations were also conducted applying the 100FC-, 0FC- and 0FCSC-scenarios to the entire tropics. The forest-cover data used in the 100FC-scenario were taken from the map of potential forest cover compiled by Billington et al. (1996). The map was amended to include areas not classified as forest originally but that are currently under forest (see Mullligan (2010) for details). As in the previous sensitivity analysis for selected tropical catchments, curve numbers pertaining to each of the four scenarios were computed by replacing the dominant forest type by grassland and vice versa for increases in forest

cover, as per the amended Billington et al. (1996) map. In addition, any decrease in forest cover was associated with a change from good to poor HSC.

2.5. Indicators of streamflow regime alterations

Three indicators based on monthly streamflow amounts were computed to identify grid cells for which the streamflow regime was altered by changes in forest cover and/or surface condition. The following indicators were computed (partly modified from Döll et al., 2009):

- The indicator for the effect of forest conversion on long-term mean annual streamflow (ILTA) computes the relative difference in long-term mean annual streamflow before and after conversion.
- The indicator for the effect of forest conversion on streamflow seasonal amplitude (ISA) computes the relative difference in long-term mean seasonal amplitude (highest monthly streamflow minus lowest monthly streamflow) before and after conversion.
- The indicator for the effect of forest conversion on low flows (ILF) computes the number of months with decreased (total) flows out of four months during the dry-season (months with lower streamflow) after conversion. In contrast to both ILTA and ISA, ILF is a categorical indicator which can assume integer values from 0 to 4, depending on the number of months with decreased flow during the dry season. A period of four months of low flows was determined for every grid cell from the corresponding long-term monthly averages. A duration of four months was chosen because in many areas the dry season lasts longer than 2 months (Foster and Chilton, 1993).

Due to uncertainties in the model input data (particularly precipitation), as well as in the predicted streamflow outputs and overall model bias, the respective indicators were interpreted mostly in relative rather than absolute terms. In addition, due to the relatively coarse scale of the analysis, the derived indicator values should be considered as first

estimates and were used mainly to identify: (i) potential 'hot spots' of hydrological change after forest conversion and soil degradation across the tropics; and (ii) the chief underlying biophysical characteristics of these 'hot spots' that render the hydrological regime of such areas vulnerable to change.

3. Results

3.1. Curve Number-related maps for tropical conditions

The Hydrological Soil Condition map (HSC) derived for the tropics as a whole is shown in Fig. 3a, while the spatial patterns for HSC and the degree of land degradation according to the RUE-adjusted trend in NDVI of Bai et al. (2008) are compared for the Republic of South Africa in Figs. 3b and 3c, respectively, showing reasonable agreement. Figure 4 depicts the corresponding map of Hydrological Soil Groups (HSG) for the tropics at large, whereas the re-sampled 1° grid-cell resolution Curve Number map is shown in Fig. 5a. Pan-tropical values of CN are normally distributed (mean ± standard deviation = 71 ± 8, n = 3743 grid cells) with 90% of the values falling between 60 and 91.As an example, the spatial variability in predicted amounts of storm runoff across the tropics for a uniformly distributed design event rainfall of 50 mm (using Eq. (2)) under current land-cover conditions is shown in Fig. 5b.

<Figure 3 about here>

<Figure 4 about here>

<Figure 5 about here>

3.2. Streamflow sensitivity analyses for selected tropical catchments

The simulated patterns of monthly streamflow (Q_{tot}) for the 235 km^2 upper Konto catchment (East Java) showed Q_{tot} and evapotranspiration (E_{tot}) to behave similarly in simulations for a given land cover (i.e., forest or grassland), regardless of any contrasts in infiltration conditions SC (Fig. 6a, b). A (very) slight reduction in Q_{tot} was observed during the dry months of June–August in the 0FCSC-scenario compared to the 100FC-case (Fig. 6a). Changes in E_{tot} for the 0FC- and 0FCSC-scenarios showed a decline during the dry season that was both delayed and petering off compared to the 100FC-scenario (Fig. 6b) indicating lowered moisture availability in the shallow-soil compartment during this time of year and causing a further reduction in grassland E_{tot} during the dry season. Nonetheless, changes in soil condition redistributed the components of Q_{tot}, such that the simulations imposing a negative change in SC gave higher storm runoff (Q_R) and lower baseflow (Q_g) (Figs. 6c and d). Furthermore, wet-season Q_{tot} (January–April) was enhanced in the two non-forest simulations (i.e. with and without SC), whereas the associated seasonal peak occurred one month earlier (Fig. 6a).

<Figure 6 about here>

In the small (3 km^2) sub-humid Babati catchment (Tanzania), changes in soil conditions proved more important than differences in vegetation cover (i.e., in E_{tot}). The two simulations with imposed negative changes in SC gave higher streamflow during wet months (January–April) than did the simulations without changed SC, regardless of forest presence or absence (Fig. 7a). Pertinently, most of the change in Q_{tot} resulted from changes in storm runoff Q_R, with a negligible effect on baseflow Q_g (Figs. 7c and d). E_{tot} almost halted in the long dry season for the 0FC-simulations (Fig. 7b) due to insufficient water storage in the shallow-soil compartment. Simulated E_{tot} was higher for grassland than for forest during wet months, but

the simulations with 100FC sustained E_{tot} throughout the dry season because of continued access of the roots to deep soil water stores (Fig. 7b).

<**Figure 7 about here**>

Vegetation cover was more important than soil conditions in the large (175,360 km^2) Tocantins river basin (Amazonia) in explaining the changes in monthly Q_{tot} and E_{tot} associated with the respective scenarios (Fig. 8). However, amounts of Q_{tot} appeared to be modulated by SC (Fig. 8a) because peak Q_{tot} occurred two months earlier in the simulations with changed SC, while flows in the initial dry season months (May–July) were slightly reduced. In the scenarios without an imposed change in SC, the results indicated a 'carry over' of water that had infiltrated during the rainy season well into the dry period in the form of sustained Q_g (Fig. 8d). Seasonal patterns of E_{tot} for the Tocantins were similar to those for the Babati area, although in the Amazonian case there was sufficient water stored in the shallow soil layer to sustain some E_{tot} for the grassland during the dry months (Fig. 8b).

<**Figure 8 about here**>

In the monsoonal but more humid upper Mahaweli catchment (1100 km^2, Sri Lanka), Q_{tot} in the 100FC-scenario was generally lower than in the simulations with 0FC (Fig. 9a), whereas E_{tot} was higher throughout the year in 100FC-simulations (Fig. 9b). The recession of Q_{tot} appeared to be controlled by SC, with faster recessions observed in the simulations involving a change in SC. Simulations with 0FC also had higher Q_{tot} during the dry months, regardless of changes in SC (Fig. 9a), although Q_g was slightly reduced relative to forested baseline conditions in the 0FCSC-scenario (Fig. 9d). Further, the seasonal peak occurred one month earlier (November versus December) in the simulations with changed SC (Fig. 9a).

<**Figure 9 about here**>

3.3. Streamflow sensitivity analysis across the tropics

For the tropics as a whole, the predicted relative change in long-term mean annual streamflow (ILTA) increased by 18% when only vegetation cover was changed (from 100FC to 0FC), whereas it increased by 26% when soil conditions were changed adversely as well (i.e. from 100FC to 0FCSC). For the 100FC to 0FC scenario (Fig. 10a), substantial increases in ILTA (>30%) were generally predicted for areas with high precipitation, but also in some areas with seasonal precipitation (e.g., the Brazilian *cerrado* zone, Madagascar, mainland Southeast Asia, Sub-Saharan East Africa, northern Australia, North-east and West India, western Mexico). Corresponding predicted increases in flows in less humid areas were less pronounced (e.g., eastern Brazil, southern Madagascar, inland Australia, central India, northern Mexico) but ILTA-values increased substantially in these drier areas after additional land degradation (100FC– 0FCSC scenario; Fig. 10b).

<Figure 10 about here>

The predicted contrasts in changes in ILTA associated with the two main scenarios (deforestation-only and deforestation plus soil degradation) under different climate conditions are illustrated in Fig. 11 as a function of the grid-cell humidity index (HI, defined as MAP/PET, with MAP being the mean annual precipitation and PET, potential evapotranspiration). Changes in ILTA for the 100FC–0FC (Fig. 11a) and 100FC–0FCSC scenarios (Fig. 11b) were more pronounced in drier areas (HI<0.9) and less marked in wetter areas (HI>1.3).

<Figure 11 about here>

The spatial patterns obtained for the changes in the seasonal (flow) amplitude indicator (ISA) corresponding with the respective scenarios were similar to those found earlier for the ILTA, although negligible change (<1%) was found for some (humid) areas in the Congo Basin and central South America under either scenario (Fig. 12). For the tropics as a whole, the average inferred change in ISA was 11% for the deforestation scenario but 20% for the deforestation plus soil degradation scenario.

<Figure 12 about here>

The results for the third indicator of streamflow change, i.e., the number of months with decreased Q_{tot} during the four months with the lowest flows (ILF), are shown only for the 100FC–0FCSC comparison (Fig. 13) as results for the 100FC–0FC scenario would be trivial (higher Q_{tot} in the 0FC-case because of reduced E_{tot} would render ILF zero throughout). The simulation results identified a number of areas with a reduction in Q_{tot} for some of the driest months, despite the associated decreases in E_{tot}. Out of the total number of 3743 grid cells, 704 cells (19%) exhibited potentially reduced low flows during at least one month (i.e. ILF ≥1). Figure 13 shows several clusters with ILF≥1, notably in Central America, northern South America, the Andes, Bolivia, Brazil, the Caribbean, Congo, Gabon, Tanzania, Ethiopia, South Africa, Madagascar, northern India, Bangladesh, as well as several countries in Southeast Asia and parts of northern Australia.

<Figure 13 about here>

To shed further light on the possible factors underlying the patterns shown in Fig. 13 for values of ILF ≥1, the distributions of selected climatic and physical characteristics (including model inputs, parameters and state variables) of two grid-cell sample populations were examined for the 100FC-simulations (i.e., before a change in forest cover): (i) all model grid cells (n = 3743, excluding semi-desert areas with an MAP <400 mm where dry-season flows

will be small to non-existent); and (ii) all grid cells with ILF≥1 (n = 704). The two populations were compared using normalised probability distribution plots (Fig. 14). Of all the climatic and physical characteristics examined, probabilistic distributions of the mean humidity index (HI), potential maximum soil water storage capacity (S_{max}), soil water content in the shallow and deep stores (S_{tot}), and groundwater recession coefficient (K_g) for the two grid-cell sample populations suggested an important difference between the two groups. In terms of climatic attributes, cells with ILF≥1 had higher HI-values (mean 1.20 ± 0.47 standard deviation) than did all modelled cells (0.70 ± 0.58) (Fig. 14a), whereas the probability distribution functions for MAP and the seasonality index SI (see Table 1 for explanation) did not differ much between the two samples (not shown).

<Figure 14 about here>

The two physical model parameters, S_{max} and K_g also had different probabilistic distributions for the two sample populations (Figs. 14b and d). The PDF of S_{max} in all model grid cells exhibited a greater skew than that for the cells with ILF≥1. This was also the case for K_g, for which the average of all model cells with ILF≥1 was 0.06 d^{-1} (corresponding to a half-time of approximately 12 days) compared to 0.11 d^{-1} (half-time of ~ 6 days) for all model grid cells. The most dissimilar PDFs were found for the state variable representing soil water content in the shallow and deep compartments (S_{tot}): while a negatively skewed and bimodal probabilistic distribution was computed for S_{tot} in all model cells with ILF≥1, which indicated wetter soil conditions throughout. A summary of cell sample statistics is given in Table 4.

<Table 4 about here>

4. Discussion

4.1. Curve Numbers for stormflow estimation under tropical conditions

The soil drainage classification used in this study is based on the FAO/UNESCO Soil Map of the World which implies certain limitations that relate not only to the scale of the map, but also to the fact that soil types with potentially different drainage characteristics were lumped together. For example, different Ferralsols or Acrisols can exhibit different drainage characteristics due to differences in clay mineralogy (Tomasella and Hodnett, 1997; Elsenbeer, 2001; Chappell et al., 2007). In general, clay mineralogy affects soil permeability because of its effects on aggregate stability and structure (Driessen et al., 2001). In addition, the FAO/UNESCO Soil Map of the World was prepared mainly for agricultural purposes and its classifications are mostly based on edaphic and pedological characteristics. Consequently, most of the detailed mapping was conducted in (lowland) agricultural areas, whereas uplands, mountains and forested areas were poorly sampled by comparison (FAO/IIASA/ISRIC/ISSCAS/JRC, 2012). However, perhaps the greatest disadvantage of the map is the qualitative nature of the information on soil hydraulic properties (Terribile et al., 2011). Despite these limitations, the FAO/UNESCO map still represents the only world-wide soil classification that provides consistent, harmonised characteristics for each soil unit (Eswaran et al., 2008). As such, it has been used in several large-scale hydrological modelling applications (e.g., Döll et al., 2003; Gudmundsson et al., 2012; Zhao et al., 2012).

The adjustment of the SCS–HSG groups to tropical conditions was necessary because the classification rules were developed for soils in the U.S.A. and mainly based on soil texture (Table 1). There are no established criteria that justify application of the same rules outside the U.S.A. For instance, based on their typically high clay contents, the generally well-drained Ferralsols (FAO soil classification, IUSS Working Group WRB, 2006) would be classified as type D or C in the USDA–SCS classification (Sartori et al., 2009).

As for the curve number values reported here (Table 2 and Fig. 5a), upon visual inspection (Fig. 5a) some CN-values appear to differ from those inferred by Hong and Adler (2008). The cause of this discrepancy may well be the fact that the HSG-classification used by Hong and Adler (2008) was based on soil texture alone whereas no distinction was made between different HSCs. For example, their inferred CN- values for forest in Amazonia and the Congo Basin (~75–95) are quite high. In terms of the prevailing land cover and soil types this would seem counterintuitive, since both areas have generally well-drained Ferralsols as the dominant soil type (FAO/UNESCO, 1977) and even for poor HSCs, their CN-values should rather range between 40 and 65 (Table 2). Conversely, the CN-values reported here are similar to values that have been validated empirically at various tropical locations (Dilshad and Peel, 1994; Descheemaeker et al., 2008; Sartori et al., 2009; cf. Yu, 2012).

4.2. Streamflow sensitivity analysis for selected tropical catchments

Patterns of total streamflow (Q_{tot}) varied between the four examined catchments, with some interesting dynamics pertaining to dry-season flows (Fig. 2 and Figs. 6–9). The imposed changes in CN-values to represent poor soil conditions in the scenarios involving surface degradation did alter rainfall infiltration and the rate of streamflow recession at the end of the wet season, such that amounts of monthly storm runoff (Q_R) increased and streamflow recessions became faster. This had an impact on dry-season flows in several of the catchments. In the upper Konto catchment (Java), the patterns (but not the magnitude) of mean seasonal Q_{tot} as simulated in the scenarios with 100% forest cover (100FC) and 0% forest cover plus a negative change in soil condition (0FCSC) were similar to the ones reported by Rijsdijk and Bruijnzeel (1991) (cf. Figs. 6a and 2a). The modelled slight reduction in dry-season flows in the 0FCSC-scenario may be ascribed to the loss of

infiltration opportunities imposed by the model parameterisation. Rijsdijk and Bruijnzeel (1991) themselves attributed the observed reduction in dry-season flows to poor soil conservation practices on rain-fed cropland (occupying ca. 33% of the catchment area) as well as to an increase in sealed surfaces (roads, settlements, footpaths, together occupying ca. 5%) which proved to be a major supplier of surface runoff (Rijsdijk et al., 2007).

The increase in modelled maximum monthly Q_{tot} during the wet season in the 0FCSC-simulations for the sub-humid Babati catchment in northern Tanzania is consistent with the reported increase in wet-season flows over time for this area (Sandström, 1995). Most of the simulated increase was due to enhanced overland flow occurrence during the wet season which was caused, in turn, by a gradual loss of bio-porosity during progressive surface degradation (Sandström, 1998). Changes in vegetation cover in this low-rainfall environment, where the natural vegetation consists of open woodland and shrub rather than tall closed forest, proved to be less important (Fig. 7).

In the large (175, 360 km^2) Amazonian Tocantins river basin, the simulated patterns (although not the exact magnitudes) of mean seasonal Q_{tot} for the 100FC- and 0FCSC-simulations were similar to the ones observed by Costa et al. (2003) (see Fig. 8a and Fig. 2b) for two periods before and after major forest conversion to grazed pasture, respectively (cf. Table 3). As in our simulations, the inferred reduction in infiltration opportunities advanced by Costa et al. (2003) was not large enough to produce a marked reduction in dry-season flows after the change in vegetation cover, although there were changes in streamflow recession rate and overall redistribution of dry-season flows (Fig. 8).

The simulation results for the upper Mahaweli catchment in Sri Lanka (Fig. 9) did not fully support the slight decrease in dry-season flows reported by Madduma Bandara (1997), although the strongly enhanced wet-season flows in the two simulations involving an adverse

change in soil hydrological conditions (Fig. 9a) were in agreement with observations (Fig. 2c). It should be noted that, in this particular case, well-managed tea plantations (not undisturbed forest) were replaced by annual cropping and home gardens without appropriate soil conservation measures (Madduma Bandara, 1997). Therefore, a more pertinent comparison would be that between the 0FC- and 0FCSC-scenarios for which indeed a slight decrease in streamflow during one dry-season month was simulated (Fig. 9a).

Naturally, the simulation results obtained for these four sample catchments are site-specific and reflect the representation of the respective hydrological processes in W3RA–LUM, the specific parameter values used in the modelling, as well as the experimental design itself (i.e., comparison of full forest presence versus complete absence of forest). With regard to the magnitude of evapotranspiration (E_{tot}), W3RA–LUM mainly considers the effects of soil water availability, since this is most likely to have the greatest impact on transpiration in seasonal tropical environments (Roberts et al., 2005; Costa et al., 2010; Kunert et al., 2017). Other factors, such as energy availability for evaporation and duration of wet-canopy conditions may play a similarly important role in more humid environments carrying rain forests (Kumagai et al., 2004; Kume et al., 2011; Holwerda et al., 2012). Some of these aspects are incorporated in W3RA–LUM through its interception evaporation routine (van Dijk, 2010a).

Sensitivity simulations for the catchments with the most pronounced precipitation seasonality (Babati and Tocantins, cf. Table 3) gave higher E_{tot} for grassland at the end of the wet season compared to the fully forested situation (Figs 7b and 8b). This may be consistent with the notion that grasses tend to adopt a less conservative water-use strategy compared to trees (Rodriguez-Iturbe and Porporato, 2004; Wolf et al., 2011; Brauman et al., 2012). Reported flux tower observations of daily mean or maximum transpiration rates are similar or

even higher for (mostly temperate) grasslands than for forests (Teuling et al., 2010) but comparable values for forest and grassland have also been obtained under tropical conditions (Wolf et al., 2011; Brauman et al., 2012). However, the eddy covariance method used in the latter studies is generally unreliable during times of precipitation and estimates of interception evaporation obtained in this way may well be too low (van Dijk et al., 2015), which may go some way towards explaining the higher E_{tot} reported for grassland at the end of the wet season. Nevertheless, in some shrub-dominated environments, such as Amazonian *cerrado* (as found in parts of the Tocantins catchment) and the sub-humid Babati catchment, the leaf area index (LAI) of grasses during the wet season is comparable to (or higher than) those of trees and shrubs, with water content in the shallow-soil compartment (down to 1 m) being strongly and positively correlated to the LAI of the grass (Waterloo et al., 1999; cf. Hoffmann et al., 2005). In our sensitivity simulations, E_{tot} for grassland (i.e. in the 0FC-scenarios) reached a minimum at the end of the dry season in the more water-limited environments, or halted altogether (e.g. at Babati; Fig. 7b). Typical *cerrado* vegetation has a grassy layer that becomes inactive during the dry season (Giambelluca et al., 2009) while the same has been observed for fire-climax grasslands in the outer tropics (Waterloo et al., 1999). For a seasonal Amazonian forest site, Negrón Juarez et al. (2007) concluded that under normal or below-normal dry-season precipitation conditions, more than 75% of E_{tot} was supplied by soil water below 1 m depth, whereas during a rainier dry season, this would be about 50%. Soil moisture found at <1 m depth was typically recharged by precipitation during the wet season (Negrón Juarez et al., 2007). Deep roots in forests are likely to become more important in maintaining high rates of E_{tot} in the dry season because of their ability to access deeper soil water during times of generally enhanced insolation levels (Nepstad et al., 1994; da Rocha et al., 2004; cf. Kunert et al., 2017). Model sensitivity to imposed deforestation (both in terms of vegetation and soil condition changes) at these sites and

elsewhere will also depend on additional factors that were not considered in W3RA–LUM at the presently used spatial and temporal resolutions (1° and 1 day, respectively), but which may be incorporated in more refined future model versions, including: sub-daily variations in cloud cover and rainfall intensity, and, especially, mosaic vegetation patterns (Bierkens, 2015), as well as variations in relief and geology that affect water retention and residence time (Chappell et al., 2007; Peña-Arancibia et al., 2010; Gleeson et al., 2011; Beck et al., 2013; Zhou et al., 2015).

4.3. Streamflow sensitivity analysis across the tropics

The previous sensitivity analyses for individual well-documented catchments suggested that the representation of relevant hydrological processes (particularly for the seasonal tropics) by W3RA–LUM, as well as its performance when predicting the direction of change upon imposed deforestation and changed soil conditions was good enough to warrant the use of the model in a broader-scale analysis spanning the entire tropics. Due to the many uncertainties in the forcing and land-cover data used, scale issues, and other processes not captured by the model (e.g. potentially negative effects of large-scale deforestation on precipitation generation or cloud water inputs (Bruijnzeel et al., 2011; Ellison et al., 2012; Ellison et al., 2017; cf. Li et al., 2018), the present results should be considered an indication of the scale of change associated with tropical forest conversion, rather than a quantitative prediction of actual change (Coe et al., 2011). Nevertheless, some striking and suggestive patterns were obtained. For example, the higher overall value obtained for the relative change in long-term mean annual streamflow (ILTA) after including an imposed negative change in soil conditions after deforestation (i.e. an average flow increase of 26% versus 18% for forest conversion only; Fig. 10), plus the correspondingly higher values for the long-term mean

seasonal amplitude (ISA) of streamflow during rainy months (Fig. 11), suggest that dry-season flows may well decrease due to deforestation and subsequent soil degradation in areas where streamflow is highly seasonal. Further support for this comes from the fact that 97% of the grid cells with a predicted decrease in Q_{tot} during at least one month in the low flow season (i.e., ILF ≥1) had a seasonal precipitation regime (i.e. a Seasonality Index SI >0.2), while 64% of the cells had a markedly seasonal regime (SI >0.6).

The statistics (Table 4) and probability distribution functions (PDF) for various physical and model parameters (Fig. 14) that were derived for grid cells showing reduced dry-season flows for at least one month (i.e. ILF ≥1) after deforestation and soil degradation provide a clear rationale for identifying the key characteristics of areas in which dry-season flows are likely to be more sensitive to deforestation impacts and subsequent surface degradation. In terms of site Humidity Index (HI), 65% of the grid cells with ILF ≥1 had an HI >1, whereas 90% had an HI >0.65. The PDF for HI was also less negatively skewed for the grid cells with ILF ≥1 than that for all model grid cells with an MAP >400 mm (Fig. 14a). In the case of seasonal climates, this surplus of rainfall over potential evapotranspiration occurs generally during the wetter 3–6 months. Some of this surplus may infiltrate (and contribute to E_{tot}) or will run off along the surface, depending on prevailing precipitation intensities and changes in soil infiltration characteristics associated with deforestation (Bruijnzeel, 2004). The distribution of S_{max} (a proxy for surface infiltration capacity and topsoil moisture retention) for grid cells with ILF ≥1 was also less negatively skewed that that for all model grid cells (Fig. 14b), suggesting better infiltration opportunities and retention in the former. Common deforestation practices in the tropics, such as mechanized forest clearing for timber harvesting and cattle ranching, or intensive agriculture cause a number of topsoil disturbances (particularly loss of organic matter, increased compaction and surface erosion), with the degree of the disturbance determining the magnitude of the reduction in infiltration capacity

and moisture retention (Alegre and Cassel, 1996; Ziegler et al., 2004; Sidle et al., 2004; Grip et al., 2005; Negishi et al., 2008; Nyberg et al., 2012). With respect to the parameter S_{tot} (representing the total amount of water stored in the soil profile), deep soils capable of storing large amounts of water (and having, by implication, better infiltration opportunities) may 'carry over' soil moisture from the wet to the dry season (or even from wet to dry years, Tomasella et al., 2008; Cheng et al., 2017). These effects are illustrated in Fig. 14 through the normalised probability functions of S_{max} and S_{tot} for all model grid cells with ILF ≥1.

The mean groundwater recession coefficient (K_g) for all grid cells with ILF ≥1 implied a half-time that was roughly twice the value obtained for all model grid cells (i.e. ca. 12 and 6 days, respectively; Table 4). The equation normally used to describe rates of baseflow recession (Peña-Arancibia et al., 2010) corresponds with the part of the hydrograph associated with prolonged periods with little or no precipitation. As such, it illustrates in a general way the nature of the groundwater storages feeding the streamflow (Tallaksen, 1995). Deep soils and permeable regoliths are widely present in tropical landscapes (Chappell et al., 2007), and their lagging effect is expected to reduce seasonal streamflow variability as well as sustain flows during the dry season. In particularly porous catchments, dry-season flows may contribute up to 30% of all streamflow (see Le Maître and Colvin (2008) for an example from temperate South Africa). In karst-dominated landscapes, as in mountainous North-west Vietnam, baseflow contributions to total streamflow can be as high as 80% (Tam et al., 2001). Notwithstanding, root-accessible storage capacity and groundwater recession parameters vary spatially in ways that are currently challenging to predict.

Structural streamflow regulation should also be considered when interpreting the spatial patterns of ILF after tropical deforestation at the scale used in our analysis (Fig. 13). Man-made reservoirs are purposely built to increase water availability during the dry season for irrigation, domestic and industrial uses, hydropower generation and/or flood protection

during rainy periods. Any adverse impacts of deforestation and soil degradation on dry-season flows in areas with regulated flow will likely be offset by the presence of dams (Döll et al., 2009; Saraiva Okello et al., 2015; Timpe and Kaplan, 2017). The effects of streamflow regulation were not yet considered in W3RA–LUM, nor were atmospheric feedbacks that may be important when the scale of deforestation is in the order of the model grid cell (10,000 km^2). The vexed question as to whether, and to what extent, land cover determines the amount of precipitation it receives has been hotly debated during the last decades (Wang and Eltahir, 2000; Makarieva and Gorshkov, 2007, 2009; Meesters et al., 2009; Angelini et al., 2011; Poveda et al., 2014) but despite progress with the description of the various interactions involved (including teleconnections; Van der Ent et al., 2010; Van der Ent et al., 2013; Makarieva et al., 2017; Li et al., 2018), there is no consensus as yet. For a recent discussion of the subject the reader is referred to Ellison et al. (2017) and Li et al. (2018).

5. Conclusions

A global hydrological model (W3RA) was tailored to assess the trade-off between changes in two opposing processes affecting dry-season flows after tropical forest conversion, i.e. the forest 'pump' effect (evapotranspiration) and the forest 'sponge' effect (infiltration and water retention). Several modifications made to the model based on the Soil Conservation Service Curve Number (CN) method accounted for surface degradation explicitly. The approach included the development of a hydrological soil condition indicator (as a proxy for soil infiltration capacity) based, in turn, on a more realistic global assessment of land degradation status derived from trends in the so-called long-term rain-use efficiency (RUE)-adjusted normalised difference vegetation index (NDVI).

The adjusted model (W3RA–LUM) was used in sensitivity experiments for four tropical catchments with documented deforestation impacts on dry-season flows. The simulated impacts of deforestation on catchment hydrological functioning allowed a better understanding of the observed streamflow patterns in the four catchments. Deforestation coupled with surface degradation (reduced infiltration) enhanced stormflow production during the wet season which affected groundwater recharge negatively, resulting in lowered baseflow. Faster rates of streamflow recession and earlier seasonal flows peaks were observed for simulations with 0% forest cover and lowered infiltration (poor soil conditions) compared to simulations with 100% forest cover and adequate infiltration (good soil conditions). Good soil conditions also appeared to dampen the seasonal variability of streamflow.

Streamflow sensitivity analyses similar to the site sensitivity experiments described above were also performed for the tropics as a whole. Deforestation scenarios gave an increase in mean annual streamflow of 26% (n = 3743 pixels of 1^{o} each) if there were concurrent changes from good to poor infiltration conditions, as opposed to 18% when infiltration conditions were maintained (i.e. forest conversion to grassland only). Relative increases in flows were more pronounced in more water-limited and seasonal environments. For some areas (n = 704 pixels or 19%), there was an inferred *reduction* in streamflow after forest conversion and reduced infiltration during some of the driest months, despite corresponding decreases in vegetation water use. Further analysis showed that forest removal and reductions in infiltration capacity tended to have a negative impact on dry-season flows in areas with: (i) strong precipitation- and streamflow seasonality; (ii) a sufficiently high surface infiltration capacity to accommodate the prevailing precipitation intensities under undisturbed conditions; (iii) sufficient precipitation in excess of potential evapotranspiration during wet months to recharge deep soil- and groundwater stores; (iv) sufficient soil water storage to

carry infiltrated wet-season rainfall over to the next dry season; and (v) a sufficiently slow groundwater recession maintaining baseflow throughout the dry season.

Areas or 'hot-spots' that showed a reduction in streamflow for some of the driest months (despite the noted decreases in vegetation water use associated with the conversion from forest to grassland) after deforestation and advanced soil degradation included: Central America, northern South America, the Andes, Bolivia, Brazil, the Caribbean, Congo, Gabon, Tanzania, Ethiopia, South Africa, Madagascar, India, Bangladesh, several countries in Southeast Asia, and northern Australia.

Acknowledgements

Microsoft Research provided a scholarship to the lead-author. CSIRO Land and Water, Conservation International, and the Andean Basin Focal Project (part of the CGIAR Challenge Programme on Water and Food) generously provided additional funds. The authors express their gratitude to Dr. Nick Chappell (Lancaster University) and Dr. Wouter Buytaert (Imperial College London) for valuable comments on an earlier draft. Dr. Lu Zhang and Dr. Lei Cheng (CSIRO Land and Water) and three anonymous reviewers provided further insightful comments.

References

Alegre, J.C., Cassel, D.K., 1996. Dynamics of soil physical properties under alternative systems to slash-and-burn. Agric. Ecosyst. Environ. 58, 39-48.

Alexandratos, N., Bruinsma, J., 2012. World agriculture towards 2030/2050: the 2012 revision. U.N. Food and Agricultural Organization ESA Working Paper no. 12-03, 147 pp (http://www.fao.org/docrep/016/ap106e/ap106e.pdf, last visited September 2018).

Angelini, I.M., Garstang, M., Davis, R.E., Hayden, B., Fitzjarrald, D.R., Legates, D.R., Greco, S., Macko, S., Connors, V., 2011. On the coupling between vegetation and the atmosphere. Theor. Appl. Climatol. 105, 243-261.

Bai, Z.G., Dent, D.L., Olsson, L., Schaepman, M.E., 2008. Proxy global assessment of land degradation. Soil Use Manage. 24, 223-234.

Batjes, N.H., 1995. A homogenized soil data file for global environmental research: A subset of FAO, ISRIC and NRCS profiles (Version 1.0). International Soil Reference and Information Centre, Wageningen, The Netherlands (https://www.isric.org/sites/default/files/isric_report_1995_10b.pdf, last visited September 2018).

Batjes, N.H., 2006. ISRIC-WISE derived soil properties on a 5 by 5 arc-minutes global grid (version 1.0). International Soil Reference and Information Centre, Wageningen, The Netherlands (https://www.isric.org/sites/default/files/isric_report_2012_01.pdf, last visited September 2018).

Beck, H.E., de Jeu, R.A.M., Schellekens, J., van Dijk, A.I.J.M., Bruijnzeel, L.A., 2009. Improving Curve Number-based storm runoff estimates using soil moisture proxies. IEEE J. Selected Topics in Appl. Earth Observ. Remote Sensing 2, 250-259.

Beck, H.E., Bruijnzeel, L.A., van Dijk, A.I.J.M., McVicar, T.R., Scatena, F.N., Schellekens, J., 2013. The impact of forest regeneration on streamflow in 12 mesoscale humid tropical catchments. Hydrol. Earth Syst. Sci. 17, 2613-2635.

Bierkens, M.F.P., 2015. Global hydrology 2015: state, trends, and directions. Water Resourc. Res. 51, 4923-4947.

Billington, C., Kapos, V., Edwards, M., Blyth, S., Iremonger, S., 1996. Estimated original forest cover map: a first attempt. World Conservation Monitoring Centre, Cambridge, U.K.

Blair, A., Sanger, D., White, D., Holland, A.F., Vandiver, L., Bowker, C., White, S., 2014. Quantifying and simulating stormwater runoff in watersheds. Hydrol. Proc. 28, 559-569.

Bonell, M., Purandara, B.K., Venkatesh, B., Krishnaswamy, J., Acharya, H.A.K., Singh, U.V., Jayakumar, R., Chappell, N., 2010. The impact of forest use and reforestation on soil hydraulic conductivity in the Western Ghats of India: Implications for surface and sub-surface hydrology. J. Hydrol. 391, 49-64.

Brauman, K.A., Freyberg, D.L., Daily, G.C., 2012. Land cover effects on groundwater recharge in the tropics: ecohydrologic mechanisms. Ecohydrology 5, 435-444.

Brown, A.E., Zhang, L., McMahon, T.A., Western, A.W., Vertessy, R.A., 2005. A review of paired catchment studies for determining changes in water yield resulting from alterations in vegetation. J. Hydrol. 310, 28-61.

Bruijnzeel, L.A., 1990. Hydrology of moist tropical forests and effects of conversion: a state of knowledge review. UNESCO International Hydrological Programme, Paris, and Free University, Amsterdam, 224 pp.

Bruijnzeel, L.A., 2004. Hydrological functions of tropical forests: not seeing the soil for the trees? Agric. Ecosyst. Environ. 104, 185-228.

Bruijnzeel, L.A., Mulligan, M., Scatena, F.N., 2011. Hydrometeorology of tropical montane cloud forests: emerging patterns. Hydrol. Proc. 25, 465-498.

Burgess, S.S.O., Adams, M.A., Turner, N.C., Ong, C.K., 1998. The redistribution of soil water by tree root systems. Oecologia 115, 306-311.

Canadell, J., Jackson, R.B., Ehleringer, J.R., Mooney, H.A., Sala, O.E., Schulze, E.D., 1996. Maximum rooting depth of vegetation types at the global scale. Oecologia 108, 583-595.

Chandler, D.G., Walter, M.F., 1998. Runoff responses among common land uses in the uplands of Matalom, Leyte, Philippines. Trans. Am. Soc. Agric. Eng. 41, 1635-1641.

Chappell, N.A., Sherlock, M., Bidin, K., Macdonald, R., Najman, Y., Davies, G., 2007. Runoff processes in Southeast Asia: role of soil, regolith, and rock type. In: Swada, H., Araki, M., Chappell, N.A., LaFrankie, J.V., Shimizu, A. (Eds.), Forest Environments in the Mekong River Basin. Springer-Verlag, Tokyo, pp. 3-23.

Cheng, Y., Ogden, F.L., Zhu, J., 2017. Earthworms and tree roots: a model study of the effect of preferential flow paths on runoff generation and groundwater recharge in steep, saprolitic tropical lowland catchments. Water Resourc. Res. 53, doi: 10.1002/2016 WR020258.

Coe, M.T., Latrubesse, E.M., Ferreira, M.E., Amsler, M.L., 2011. The effects of deforestation and climate variability on the streamflow of the Araguaia River, Brazil. Biogeochem. 105, 119-131.

Costa, M.H., Botta, A., Cardille, J.A., 2003. Effects of large-scale changes in land cover on the discharge of the Tocantins River, Southeastern Amazonia. J. Hydrol. 283, 206-217.

Costa, M.H., Biajoli, M.C., Sanches, L., Malhado, A.C.M., Hutyra, L.R., da Rocha, H.R., Aguiar, R.G., de Araujo, A.C., 2010. Atmospheric versus vegetation controls of Amazonian tropical rain forest evapotranspiration: are the wet and seasonally dry rain forests any different? J. Geophys. Res.-Biogeosci. 115, G4. https://doi.org/10.1029/2009JG001179.

da Rocha, H.R., Goulden, M.L., Miller, S.D., Menton, M.C., Pinto, L., de Freitas, H.C., Figueira, A., 2004. Seasonality of water and heat fluxes over a tropical forest in eastern Amazonia. Ecol. Applic. 14, S22-S32.

Descheemaeker, K., Poesen, J., Borselli, L., Nyssen, J., Raes, D., Haile, M., Muys, B., Deckers, J., 2008. Runoff curve numbers for steep hillslopes with natural vegetation in semi-arid tropical highlands, northern Ethiopia. Hydrol. Proc. 22, 4097-4105.

Dilshad, M., Peel, L.J., 1994. Evaluation of the USDA curve number method for agricultural catchments in the Australian semiarid tropics. Austral. J. Soil Res. 32, 673-685.

Döll, P., Fiedler, K., Zhang, J., 2009. Global-scale analysis of river flow alterations due to water withdrawals and reservoirs. Hydrol. Earth Syst. Sci. 13, 2413-2432.

Döll, P., Kaspar, F., Lehner, B., 2003. A global hydrological model for deriving water availability indicators: model tuning and validation. J. Hydrol. 270, 105-134.

Driessen, P., Deckers, J., Spaargaren, O., Nachtergaele, F., 2001. Lecture notes on the major soils of the world. FAO, Rome (http://www.fao.org/3/a-y1899e.pdf, last visited September 2018)

El-Hames, A.S., 2012. An empirical method for peak discharge prediction in ungauged arid and semi-arid region catchments based on morphological parameters and SCS curve number. J. Hydrol. 456-457, 94-100.

Ellison, D., Futter, M.N., Bishop, K., 2012. On the forest cover-water yield debate: from demand- to supply-side thinking. Global Change Biol. 18, 806-820.

Ellison, D., Morris, C.E., Locatelli, B., Sheil, D., Cohen, J., Murdiyarso, D., Gutierrez, V., van Noordwijk, M., Creed, I.F., Pokorny, J., Gaveau, D., Spracklen, D.V., Tobella, A.B., Ilstedt, U., Teuling, A.J., Gebrehiwot, S.G., Sands, D.C., Muys, B., Verbist, B., Springgay, E., Sugandi, Y., Sullivan, C.A., 2017. Trees, forests and water: cool insights for a hot world. Global Environ. Change 43, 51-61.

Elsenbeer, H., 2001. Hydrologic flowpaths in tropical rainforest soilscapes - a review. Hydrol. Proc. 15, 175-759.

Eswaran, H., Rice, T., Ahrens, R., Stewart, B.A., 2008. Soil Classification: A Global Desk Reference. CRC Press, Boca Raton, Florida, U.S.A.

FAO, 2006. Global Forest Resources Assessment 2005, Main Report. Progress Towards Sustainable Forest Management FAO Forestry paper 147, Rome, 320 pp.

FAO/IIASA/ISRIC/ISSCAS/JRC, 2012. Harmonized World Soil Database (version 1.2). FAO. Rome, Italy and IIASA, Laxenburg, Austria (http://www.fao.org/soils-portal/soil-survey/soil-maps-and-databases/harmonized-world-soil-database-v12/en/, last visited September 2018).

FAO-UNESCO, 1977. Soil Map of the World. FAO, Rome and UNESCO, Paris (http://www.fao.org/docrep/019/as352e/as352e.pdf, last visited September 2018).

Farley, K.A., Jobbággy, E., Jackson, R.B., 2005. Effects of afforestation on water yield: a global synthesis with implications for policy. Global Change Biol. 11, 1565–1576.

Foster, S.D.D., Chilton, P.J., 1993. Groundwater systems in the humid tropics. In: Bonell, M., Hufschmidt, M.M., Gladwell, J.S. (Eds.), Hydrology and Water Management in the Tropics. Cambridge University Press, Cambridge, U.K., pp. 261-272.

Frost, A. J., Ramchurn, A., Smith, A. 2016. The Bureau's Operational AWRA Landscape (AWRA-L) Model. Bureau of Meteorology Technical Report (available at http://www.bom.gov.au/water/landscape/assets/static/publications/Frost__Model_Description_Report.pdf, last visited October 2018).

Germer, S., Neill, C., Vetter, T., Chaves, J., Krusche, A.V., Elsenbeer, H., 2009. Implications of long-term land-use change for the hydrology and solute budgets of small catchments in Amazonia. J. Hydrol. 364, 349-363.

Ghimire, C.P., Bonell, M., Bruijnzeel, L.A., Coles, N.A., Lubczynski, M.W., 2013. Reforesting severely degraded grassland in the Lesser Himalaya of Nepal: effects on

soil hydraulic conductivity and overland flow production. J Geophys Res-D118, 2528-2545.

Ghimire, C.P., Bruijnzeel, L.A., Bonell, M., Coles, N., Lubczynski, M.W., Gilmour, D.A., 2014. The effects of sustained forest use on hillslope soil hydraulic conductivity in the Middle Mountains of Central Nepal. Ecohydrology 7, 478-495.

Giambelluca, T.W., Scholz, F.G., Bucci, S.J., Meinzer, F.C., Goldstein, G., Hoffmann, W.A., Franco, A.C., Buchert, M.P., 2009. Evapotranspiration and energy balance of Brazilian savannas with contrasting tree density. Agric. For. Meteor. 149, 1365-1376.

Gibbs, H.K., Ruesch, A.S., Achard, F., Clayton, M.K., Holmgren, P., Ramankutty, N., Foley, J.A., 2010. Tropical forests were the primary sources of new agricultural land in the 1980s and 1990s. Proc. Nat. Acad. Sci. U.S.A. (PNAS) 107, 16732-16737.

Gibbs, H.K., Salmon, J.M., 2015. Mapping the world's degraded lands. Appl. Geog. 57, 12-21.

Gleeson, T., Smith, L., Moosdorf, N., Hartmann, J., Durr, H.H., Manning, A.H., van Beek, L.P.H., Jellinek, A.M., 2011. Mapping permeability over the surface of the Earth. Geophys. Res. Letters 38, L02401. DOI: 10.1029/2010GL045565

Global Soil Data Task Force, 2000. Global Gridded Surfaces of Selected Soil Characteristics (IGBP-DIS) (https://daac.ornl.gov/SOILS/guides/igbp-surfaces.html, last visited September 2018).

Gordon, L.J., Steffen, W., Jonsson, B.F., Folke, C., Falkenmark, M., Johannessen, A., 2005. Human modification of global water vapor flows from the land surface. Proc. Nat. Acad. Sci. U.S.A. (PNAS) 102, 7612-7617.

Grip, H., Fritsch, J.M., Bruijnzeel, L.A., 2005. Soil and water impacts during forest conversion and stabilisation to new land use. In: Bonell, M., Bruijnzeel, L.A. (Eds.), Forests, Water and People in the Humid Tropics. Cambridge University Press, Cambridge, U.K., pp. 561-589.

Gudmundsson, L., Tallaksen, L.M., Stahl, K., Clark, D.B., Dumont, E., Hagemann, S., Bertrand, N., Gerten, D., Heinke, J., Hanasaki, N., Voss, F., Koirala, S., 2012. Comparing large-scale hydrological model simulations to observed runoff percentiles in Europe. J. Hydrometeor. 13, 604-620.

Guerschman, J.P., Van Dijk, A.I.J.M., Mattersdorf, G., Beringer, J., Hutley, L.B., Leuning, R., Pipunic, R.C., Sherman, B.S., 2009. Scaling of potential evapotranspiration with MODIS data reproduces flux observations and catchment water balance observations across Australia. J. Hydrol. 369, 107-119.

Hansen, M.C., Defries, R.S., Townshend, J.R.G., Sohlberg, R., 2000. Global land cover classification at 1km spatial resolution using a classification tree approach. Int. J. Remote Sens. 21, 1331-1364.

Hansen, M.C., DeFries, R.S., Townshend, J.R.G., Carroll, M., Dimiceli, C., Sohlberg, R.A., 2003. Global percent tree cover at a spatial resolution of 500 meters: first results of the MODIS vegetation continuous fields algorithm. Earth Interactions 7-010. https://doi.org/10.1175/1087-3562(2003)007<0001:GPTCAA>2.0.CO;2

Hawkins, R.H., Ward, T.J., Woodward, D.E., Van Mullen, J.A., 2009. Curve Number Hydrology: State of the Practice. American Society of Civil Engineers, Reston, Virginia, U.S.A.

Hoffmann, W.A., da Silva, E.R., Machado, G.C., Bucci, S.J., Scholz, F.G., Goldstein, G., Meinzer, F.C., 2005. Seasonal leaf dynamics across a tree density gradient in a Brazilian savanna. Oecologia 145, 307-316.

Holwerda, F., Bruijnzeel, L.A., Scatena, F.N., Vugts, H.F., Meesters, A.G.C.A., 2012. Wet-canopy evaporation from a Puerto Rican lower montane rain forest: the importance of realistically estimated aerodynamic conductance. J. Hydrol. 414, 1-15.

Hong, Y., Adler, R.F., 2008. Estimation of global SCS curve numbers using satellite remote sensing and geospatial data. Int. J. Remote Sens. 29, 471-477.

Hou, J.W., van Dijk, A.I.J.M., Renzullo, L.J., Vertessy, R.A., 2018. Using modelled discharge to develop satellite-based river gauging: a case study for the Amazon Basin. Hydrology and Earth System Sciences, 22(12): 6435-6448. DOI:10.5194/hess-22-6435-2018

Hou, Y., Zhang, M., Meng, Z., Liu, S., Sun, P., Yang, T., 2018. Assessing the impact of forest change and climate variability on dry season runoff by an improved single watershed approach: a comparative study in two large watersheds, China. Forests 2018, 9, 46, doi:10.3390/f9010046

IUSS Working Group WRB, 2006. World Reference Base for Soil Resources 2006, 2nd Ed. FAO, Rome (http://www.fao.org/3/a-a0510e.pdf, last visited October 2018).

Jiang, X.J., Liu, W.J., Wu, J.N., Wang, P.Y., Liu, C.G., Yuan, Z.Q., 2017. Land degradation controlled and mitigated by rubber-based agroforestry systems through optimizing soil physical conditions and water supply mechanisms: a case study in Xishuangbanna, China. Land Degrad. Dev. 28, 2277-2289.

Khaki, M. et al., 2018. Determining water storage depletion within Iran by assimilating GRACE data into the W3RA hydrological model. Advances in Water Resources, 114: 1-18. DOI:10.1016/j.advwatres.2018.02.008

Krishnaswamy, J., Bonell, M., Venkatesh, B., Purandara, B.K., Lele, S., Kiran, M.C., Reddy, V., Badiger, S., Rakesh, K.N., 2012. The rain-runoff response of tropical humid forest ecosystems to use and reforestation in the Western Ghats of India. J. Hydrol. 472, 216-237.

Krishnaswamy, J., Bonell, M., Venkatesh, B., Purandara, B.K., Rakesh, K.N., Lele, S., Kiran, M.C., Reddy, V., Badiger, S., 2013. The groundwater recharge response and hydrologic services of tropical humid forest ecosystems to use and reforestation: support for the "infiltration-evapotranspiration trade-off hypothesis". J. Hydrol. 498, 191-209.

Kumagai, T., Katul, G.G., Saitoh, T.M., Sato, Y., Manfroi, O.J., Morooka, T., Ichie, T., Kuraji, K., Suzuki, M., Porporato, A., 2004. Water cycling in a Bornean tropical rain forest under current and projected precipitation scenarios. Water Resourc. Res. 40, W01104.

Kume, T., Tanaka, N., Kuraji, K., Komatsu, H., Yoshifuji, N., Saitoh, T.M., Suzuki, M., Kumagai, T., 2011. Ten-year evapotranspiration estimates in a Bornean tropical rainforest. Agric. For. Meteor. 151, 1183-1192.

Kunert, N., Aparecido, L.M.T., Wolff, S., Higuchi, N., dos Santos, J., de Araujo, A.C., Trumbore, S., 2017. A revised hydrological model for the Central Amazon: the importance of emergent canopy trees in the forest water budget. Agric. For. Meteor. 239, 47-57.

Lacombe, G., Ribolzi, O., de Rouw, A., Pierret, A., Latsachak, K., plus 12 others. 2016. Contradictory hydrological impacts of afforestation in the humid tropics evidenced by long-term field monitoring and simulation modelling. Hydrol. Earth Syst. Sci. 20, 2691-2704.

Le Maître, D.C., Colvin, C.A., 2008. Assessment of the contribution of groundwater discharges to rivers using monthly flow statistics and flow seasonality. Water SA 34, 549-564.

Li, Y., Piao, S., Li, L.Z.X., Chen, A., Wang, X., Ciais, P., Huang, L., Lian, X., Peng, S., Zeng, Z., Wang, K., Zhou, L., 2018. Divergent hydrological response to large-scale afforestation and vegetation greening in China. Sci. Adv. 2018, 4, eaard4182

Liu, W.J., Liu, W.Y., Lu, H.J., Duan, W.P., Li, H.M., 2011. Runoff generation in small catchments under a native rain forest and a rubber plantation in Xishuangbanna, southwestern China. Water Environ. J. 25, 138-147.

Liu, W.F., Wei, X.H., Fan, H.B., Guo, X.M., Liu, Y.Q., Zhang, M.F., Li, Q., 2015. Response of flow regimes to deforestation and reforestation in a rain-dominated large watershed of subtropical China. Hydrol. Proc. 29, 5003-5015.

Lyon, S.W., King, K., Polpanich, O.U., Lacombe, G., 2017. Assessing hydrologic changes across the Lower Mekong Basin. J. Hydrol.: Regional Studies 12, 303-314.

Madduma-Bandara, C.M., 1997. Land-use changes and tropical stream hydrology: some observations from the upper Mahaweli basin of Sri Lanka. In: Stoddard, D.R. (Ed.), Process and Form in Geomorphology. Routledge, London, pp. 175-186.

Mahé, G., Paturel, J.E., Servat, E., Conway, D., Dezetter, A., 2005. The impact of land use change on soil water holding capacity and river flow modelling in the Nakambe River, Burkina-Faso. J. Hydrol. 300, 33-43.

Makarieva, A.M., Gorshkov, V.G., 2007. Biotic pump of atmospheric moisture as driver of the hydrological cycle on land. Hydrol. Earth Syst. Sci. 11, 1013-1033.

Makarieva, A.M., Gorshkov, V.G., 2009. Reply to A. G. C. A. Meesters et al.'s comment on 'Biotic pump of atmospheric moisture as driver of the hydrological cycle on land'. Hydrol. Earth Syst. Sci. 13, 1307-1311.

Makarieva, A.M., Gorshkov, V.G., Nefiodov, A.V., Chikunov, A.V., Sheil, D., Nobre, A.D., Li, B.L., 2017. Fuel for cyclones: The water vapor budget of a hurricane as dependent on its movement. Atmosph. Res. 193, 216-230.

Martinez, L.J., Zinck, J.A., 2004. Temporal variation of soil compaction and deterioration of soil quality in pasture areas of Colombian Amazonia. Soil Tillage Res. 75, 3-17.

Meesters, A.G.C.A., Dolman, A.J., Bruijnzeel, L.A., 2009. Comment on 'Biotic pump of atmospheric moisture as driver of the hydrologic cycle on land' by A.M. Makarieva and V.G. Gorshkov, *Hydrol. Earth Syst. Sci.* 11, 1013-1033. Hydrol. Earth Syst. Sci. 13, 1299-1305.

Mehta, V.K., Sullivan, P.J., Walter, M.T., Krishnaswamy, J., DeGloria, S.D., 2008. Impacts of disturbance on soil properties in a dry tropical forest in Southern India. Ecohydrology 1, 161-175.

Mishra, S.K., Singh, V.P., 2003. Soil Conservation Service Curve Number (SCS-CN) Methodology. Springer Verlag, Berlin, 516 pp.

Mishra, V., Cherkauer, K.A., Niyogi, D., Lei, M., Pijanowski, B.C., Ray, D.K., Bowling, L.C., Yang, G., 2010. A regional scale assessment of land use/land cover and climatic changes on water and energy cycle in the upper Midwest United States. Int. J. Climatol. 30, 2025-2044.

Moody, E.G., King, M.D., Platnick, S., Schaaf, C.B., Gao, F., 2005. Spatially complete global spectral surface albedos: value-added datasets derived from terra MODIS land products. IEEE Trans. Geosci. Remote Sens. 43, 144-158.

Mullligan, M., 2010. Modelling the tropics-wide extent and distribution of cloud forest and cloud forest loss, with implications for conservation priority. In: Bruijnzeel, L.A., Scatena, F.N., Hamilton, L.S. (Eds.), Tropical Montane Cloud Forests. Cambridge University Press, Cambridge, U.K., pp. 14-38.

Mulligan, M., Burke, S.M., 2005. FIESTA: Fog Interception for the Enhancement of Streamflow in Tropical Areas. AMBIOTEK, Leigh-on-Sea, U.K. (http://www.ambiotek.com/fiesta/FIESTA_ftr_ambiotek_final.pdf, last visited October 2018)

Negishi, J.N., Sidle, R.C., Ziegler, A.D., Noguchi, S., Rahim, N.A., 2008. Contribution of intercepted subsurface flow to road runoff and sediment transport in a logging-disturbed tropical catchment. Earth Surf. Proc. and Landforms 33, 1174-1191.

Negrón Juarez, R.I., Hodnett, M.G., Fu, R., Goulden, M.L., von Randow, C., 2007. Control of dry season evapotranspiration over the Amazonian forest as inferred from observations at a southern Amazon forest site. J. Climate 20, 2827-2839.

Nepstad, D.C., Decarvalho, C.R., Davidson, E.A., Jipp, P.H., Lefebvre, P.A., Negreiros, G.H., Dasilva, E.D., Stone, T.A., Trumbore, S.E., Vieira, S., 1994. The role of deep roots in the hydrological and carbon cycles of Amazonian forests and pastures. Nature 372, 666-669.

Nyberg, G., Tobella, A.B., Kinyangi, J., Ilstedt, U., 2012. Soil property changes over a 120-yr chronosequence from forest to agriculture in western Kenya. Hydrol. Earth Syst. Sci. 16, 2085-2094.

Ogden, F.L., Crouch, T.D., Stallard, R.F., Hall, J.S., 2013. Effect of land cover and use on dry season river runoff, runoff efficiency, and peak storm runoff in the seasonal tropics of Central Panama. Water Resourc. Res. 49, 8443-8462.

Ogden, F.L., Hawkins, R., Walter, M.T., Goodrich, D.C., 2017. Comment on "Beyond the SCS-CN method: A theoretical framework for spatially lumped rainfall-runoff response" by M. S. Bartlett et al. Water Resourc. Res. 53, 6345-6350.

Peña-Arancibia, J.L., van Dijk, A.I.J.M., Mulligan, M., Bruijnzeel, L.A., 2010. The role of climatic and terrain attributes in estimating baseflow recession in tropical catchments. Hydrol. Earth Syst. Sci. 14, 2193-2205.

Ponce, V.M., Hawkins, R.H., 1996. Runoff Curve Numbers: has it reached maturity? J. Hydrol. Eng. 1, 11-19.

Poveda, G., Jaramillo, L., Vallejo, L.F., 2014. Seasonal precipitation patterns along pathways of South American low-level jets and aerial rivers. Water Resourc. Res. 50, 98-118, DOI:2013WR014087

Qazi, N.Q., Bruijnzeel, L.A., Rai, S.P., Ghimire, C.P., 2017. Impact of forest degradation on streamflow regime and runoff response to rainfall in the Garhwal Himalaya, Northwest India. Hydrol. Sci. J. 62, 1114-1130.

Recha, J.W., Lehmann, J., Walter, M.T., Pell, A., Verchot, L., Johnson, M., 2012. Stream discharge in tropical headwater catchments as a result of forest clearing and soil degradation. Earth Interactions 16–013, DOI:10.1175/2012EI000439.1.

Rijsdijk A, Bruijnzeel LA. 1991. Erosion, sediment yield and land use patterns in the upper Konto watershed, East Java, Indonesia. Part III. Results of the 1989–1990 measuring campaign. Konto River Project Communication 18. DHV Consultants, Amersfoort, the Netherlands, 59 p.

Rijsdijk, A., Bruijnzeel, L.A.S., Sutoto, C.K., 2007. Runoff and sediment yield from rural roads, trails and settlements in the upper Konto catchment, East Java, Indonesia. Geomorphol. 87, 28-37.

Roa-García, M.C., Brown, S., Schreier, H., Lavkulich, L.M., 2011. The role of land use and soils in regulating water flow in small headwater catchments of the Andes. Water Resourc. Res. 47, W05510.

Roberts, J.M., Gash, J.H.C., Tani, M., Bruijnzeel, L.A., 2005. Controls on evaporation in lowland tropical rainforest. In: Bonell, M., Bruijnzeel, L.A. (Eds.), Water and People in the Humid Tropics. Cambridge University Press, Cambridge, U.K., pp. 287-313.

Rodriguez, D.A., Tomasella J, Linhares, C., 2010. Is the forest conversion to pasture affecting the hydrological response of Amazonian catchments? Signals in the Ji-Paraná Basin. Hydrol. Proc. 24, 1254-1269.

Rodriguez-Iturbe, I., Porporato, A., 2004. Ecohydrology of Water-Controlled Ecosystems: Soil Moisture and Plant Dynamics. Cambridge University Press,Cambridge, U.K., 464 p.

Sandström K, 1995. Forest and water–friends or foes? Hydrological implications of deforestation and land degradation in semi-arid Tanzania. Ph.D. Dissertation, Linkoping University, Linkoping, Sweden, 120 pp.

Sandström, K., 1998. Can forests "provide" water: widespread myth or scientific reality? Ambio 27, 132-138.

Saraiva Okello, A.M.L., Masih, I., Uhlenbrook, S., Jewitt, G.P.W., van der Zaag, P., Riddell, E., 2015. Drivers of spatial and temporal variability of streamflow in the Incomati River Basin. Hydrol. Earth Syst. Sci. 19, 657-673.

Sartori, A., Maia Genovez, A., Lombardi Neto, F., 2009. Tentative hydrologic soil classification for tropical soils. Advances in Water Resources and Hydraulic Engineering: Proceedings of 16th IAHR-APD Congress and 3rd Symposium of IAHR-ISHS. Springer Verlag, Berlin, pp. 199-204.

Schaake, J.C., Koren, V.I., Duan, Q.Y., Mitchell, K., Chen, F., 1996. Simple water balance model for estimating runoff at different spatial and temporal scales. J. Geophys. Res.-Atm. 101, 7461-7475.

Schenk, H.J., Jackson, R.B., 2002. The global biogeography of roots. Ecol. Monogr. 72, 311-328.

Sheffield, J., Goteti, G., Wood, E.F., 2006. Development of a 50-year high-resolution global dataset of meteorological forcings for land surface modeling. J. Climate 19, 3088-3111.

Sidle, R.C., Sasaki, S., Otsuki, M., Noguchi, S., Nik, A.R., 2004. Sediment pathways in a tropical forest: effects of logging roads and skid trails. Hydrol. Proc. 18, 703-720.

Stednick, J.D., 1996. Monitoring the effects of timber harvest on annual water yield. J. Hydrol. 176, 79-95.

Tallaksen, L.M., 1995. A review of baseflow recession analysis. J. Hydrol. 165, 349-370.

Tam, V.T., Vu, T.M.N., Batelaan, O., 2001. Hydrogeological characteristics of a karst mountainous catchment in the northwest of Vietnam. Acta Geol. Sinica-English Ed. 75, 260-268.

Terribile, F., Coppola, A., Langella, G., Martina, M., Basile, A., 2011. Potential and limitations of using soil mapping information to understand landscape hydrology. Hydrol. Earth Syst. Sci. 15, 3895-3933.

Teuling, A.J., Seneviratne, S.I., Stoeckli, R., Reichstein, M., Moors, E., Ciais, P., Luyssaert, S., van den Hurk, B., Ammann, C., Bernhofer, C., Dellwik, E., Gianelle, D., Gielen, B., Gruenwald, T., Klumpp, K., Montagnani, L., Moureaux, C., Sottocornola, M., Wohlfahrt, G., 2010. Contrasting response of European forest and grassland energy exchange to heatwaves. Nature Geosci. 3, 722-727.

Tian, S.Y., Van Dijk, A.I.J.M., Tregoning, P., Renzullo, L.J., 2019. Forecasting dryland vegetation condition months in advance through satellite data assimilation. Nat Commun, 10. DOI:ARTN 46910.1038/s41467-019-08403-x

Timpe, K., Kaplan, D., 2017. The changing hydrology of a dammed Amazon. Sci. Adv. 3 (11), e1700611.

Tomasella, J., Hodnett, M.G., 1997. Estimating unsaturated hydraulic conductivity of Brazilian soils using soil-water retention data. Soil Sci. 162, 703-712.

Tomasella, J., Hodnett, M.G., Cuartas, L.A., Nobre, A.D., Waterloo, M.J., Oliveira, S.M., 2008. The water balance of an Amazonian micro-catchment: the effect of interannual variability of rainfall on hydrological behaviour. Hydrol. Proc. 22, 2133-2147.

Toohey, R.C., Boll, J., Brooks, E.S., Jones, J.R., 2018. Effects of land use on soil properties and hydrological processes at the point, plot, and catchment scale in volcanic soils near Turrialba, Costa Rica. Geoderma 315, 138-148.

Trabucco, A., Zomer, R.J., Bossio, D.A., van Straaten, O., Verchot, L.V., 2008. Climate change mitigation through afforestation/reforestation: a global analysis of hydrologic impacts with four case studies. Agric. Ecosyst. Environ. 126, 81-97.

USDA-SCS, 1985. Section 4 - Hydrology. National Engineering Handbook. US Department of Agriculture, Soil Conservation Service, Washington, D.C.

Van der Ent, R.J., Savenije, H.H.G., Schaefli, B., Steele-Dunne, S.C., 2010. Origin and fate of atmospheric moisture over continents. Water Resourc. Res. 46, DOI:W09525.

Van der Ent, R.J., Tuinenburg, O.A., Knoche, H.R., Kunstmann, H., Savenije, H.H.G., 2013. Should we use a simple or complex model for moisture recycling and atmospheric moisture tracking? Hydrol. Earth Syst. Sci. 17, 4869-4884.

Van Dijk, A.I.J.M., 2010a. AWRA Technical Report 3. Landscape Model (version 0.5) Technical Description. WIRADA/CSIRO Water for a Healthy Country Flagship,

Canberra (http://www.clw.csiro.au/publications/waterforahealthycountry/2010/wfhc-aus-water-resources-assessment-system.pdf, last visited October 2018).

Van Dijk, A.I.J.M., 2010b. Climate and terrain factors explaining streamflow response and recession in Australian catchments. Hydrol. Earth Syst. Sci. 14, 159-169.

Van Dijk, A. I. J. M., 2010c. Selection of an appropriately simple storm runoff model. Hydrol. Earth Syst. Sci.14, 447-458.

Van Dijk, A.I.J.M., Hairsine, P.B., Peña-Arancibia, J.L., Dowling, T.I., 2007. Reforestation, water availability and stream salinity: a multi-scale analysis in the Murray-Darling Basin, Australia. For. Ecol. Manage. 251, 94-109.

Van Dijk, A.I.J.M., Peña-Arancibia, J.L., Wood, E.F., Sheffield, J., Beck, H.E., 2013. Global analysis of seasonal streamflow predictability using an ensemble prediction system and observations from 6192 small catchments worldwide. Water Resourc. Res. 49, 2729-2746.

Van Dijk, A.I.J.M. et al., 2018. Global 5 km resolution estimates of secondary evaporation including irrigation through satellite data assimilation. Hydrology and Earth System Sciences, 22(9): 4959-4980. DOI:10.5194/hess-22-4959-2018

Van Noordwijk, M., Tanika, L., Lusiana, B., 2017a. Flood risk reduction and flow buffering as ecosystem services - Part 1: Theory on flow persistence, flashiness and base flow. Hydrol Earth Syst. Sci. 21, 2321-2340.

Van Noordwijk, M., Tanika, L., Lusiana, B., 2017b. Flood risk reduction and flow buffering as ecosystem services - Part 2: Land use and rainfall intensity effects in Southeast Asia. Hydrol Earth Syst. Sci. 21, 2341-2360.

Wang, G.L., Eltahir, E.A.B., 2000. Role of vegetation dynamics in enhancing the low-frequency variability of the Sahel rainfall. Water Resourc. Res. 36, 1013-1021.

Wang, X., Liu, T., Yang, W., 2012. Development of a robust runoff-prediction model by fusing the Rational Equation and a modified SCS-CN method. Hydrol. Sci. J. 57, 1118-1140 .

Ward, R.C., 1984. On the response to precipitation of headwater streams in humid areas. J. Hydrol. 74, 171-189.

Waterloo, M.J., Bruijnzeel, L.A., Vugts, H.F., Rawaqa, T.T., 1999. Evaporation from *Pinus caribaea* plantations on former grassland soils under maritime tropical conditions. Water Resourc. Res. 35, 2133-2144.

Wolf, S., Eugster, W., Majorek, S., Buchmann, N., 2011. Afforestation of tropical pasture only marginally affects ecosystem-scale evapotranspiration. Ecosystems 14, 1264-1275.

Yu, B., 1998. Theoretical justification of SCS method for runoff estimation. J. Irrig. Drainage Eng.-ASCE 124, 306-310.

Yu, B.F., 2012. Validation of SCS Method for runoff estimation. J. Hydrol. Eng. 17, 1158-1163.

Zeng, Z.Y., Tang, G.Q., Hong, Y., Zeng, C., Yang, Y., 2017. Development of an NRCS curve number global dataset using the latest geospatial remote sensing data for worldwide hydrologic applications. Remote Sens. Letters 8, 528-536.

Zhang, L., Dawes, W.R., Walker, G.R., 2001. Response of mean annual evapotranspiration to vegetation changes at catchment scale. Water Resourc. Res. 37, 701-708.

Zhang, M., Liu M., Harper, R., Li, Q., Liu, K., Wei, X., Ning, D., Hou, Y., Liu, S., 2017. A global review on hydrological responses to forest change across multiple spatial scales: Importance of scale, climate, forest type and hydrological regime. J. Hydrol. 546, 44-59.

Zhao, F., Chiew, F.H.S., Zhang, L., Vaze, J., Perraud, J.-M., Li, M., 2012. Application of a macroscale hydrologic model to estimate streamflow across Southeast Australia. J. Hydrometeor. 13, 1233-1250.

Zhou, G., Wei, X., Luo, Y., Zhang, M., Li, Y., Qiao, Y., Liu, H., Wang, C., 2010. Forest recovery and river discharge at the regional scale of Guangdong Province, China. Water Resourc. Res. 46. DOI: 2009WR008829.

Zhou, G.Y., Wei, X., Chen, X., Zhou, P., Liu, X., Xiao, Y., Sun, G., Scott, D.F., Zhou, S., Han, L., Su, Y., 2015. Global pattern for the effect of climate and land cover on water yield. Nature Comm. 6: 5918. DOI: 10.1038/ncomms6918.

Ziegler, A.D., Fox, J.M., Xu, J.C., 2009. The Rubber juggernaut. Science 324, 1024-1025.

Ziegler AD, Giambelluca TW, Tran LT, Vana TT, Nullet MA, Fox J, Vien TD, Pinthong J, Maxwell JF, Evett S. 2004. Hydrological consequences of landscape fragmentation in mountainous northern Vietnam: evidence of accelerated overland flow generation. J. Hydrol. 287, 124–146.

Ziegler, A.D., Negishi, J., Sidle, R.C., Preechapanya, P., Sutherland, R.A., Giambelluca, T.W., Jaiaree, S., 2006. Reduction of stream sediment concentration by a riparian buffer: filtering of road runoff in disturbed headwater basins of montane mainland Southeast Asia. J. Environ. Qual. 35, 151-162.

Zimmermann, B., Papritz, A., Elsenbeer, H., 2010. Asymmetric response to disturbance and recovery: changes of soil permeability under forest-pasture-forest transitions. Geoderma 159, 209-215.

Zwartendijk, B.W., van Meerveld, H.J., Ghimire, C.P., Bruijnzeel, L.A., Ravelona, M., Jones, J.P.G., 2017. Rebuilding soil hydrological functioning after swidden agriculture in eastern Madagascar. Agric. Ecosyst. Environ. 239, 101-111.

Declaration of interests

☒ The authors declare that they have no known competing financial interests or personal relationships that could have appeared to influence the work reported in this paper.

☐The authors declare the following financial interests/personal relationships which may be considered as potential competing interests:

Figures

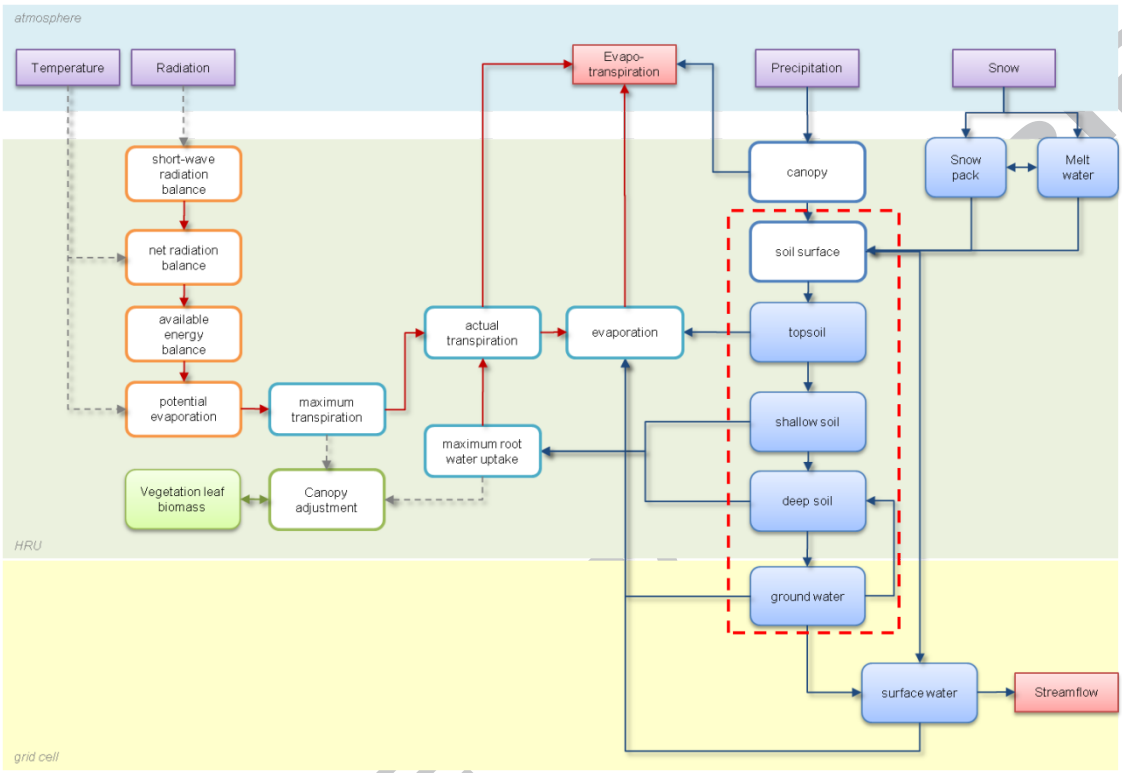

Figure 1. Flux diagram of the W3RA-LUM model structure (modified from Van Dijk, 2010a): the minimum input data requirements (purple boxes); fluxes lost from the grid cell (red boxes); water fluxes (blue arrows); energy and vapour fluxes (red arrows); functional relationships (dashed grey arrows); water balance model components described (blue rounded boxes); the surface radiation and energy balance (orange); vapour fluxes (cyan); and vegetation phenology (green). Solid blue and green colours represent dynamic model states updated from one time step to the next; outlined boxes represent transformations and partitioning. Enclosed in the red dashed box are the components of the model that were modified here.

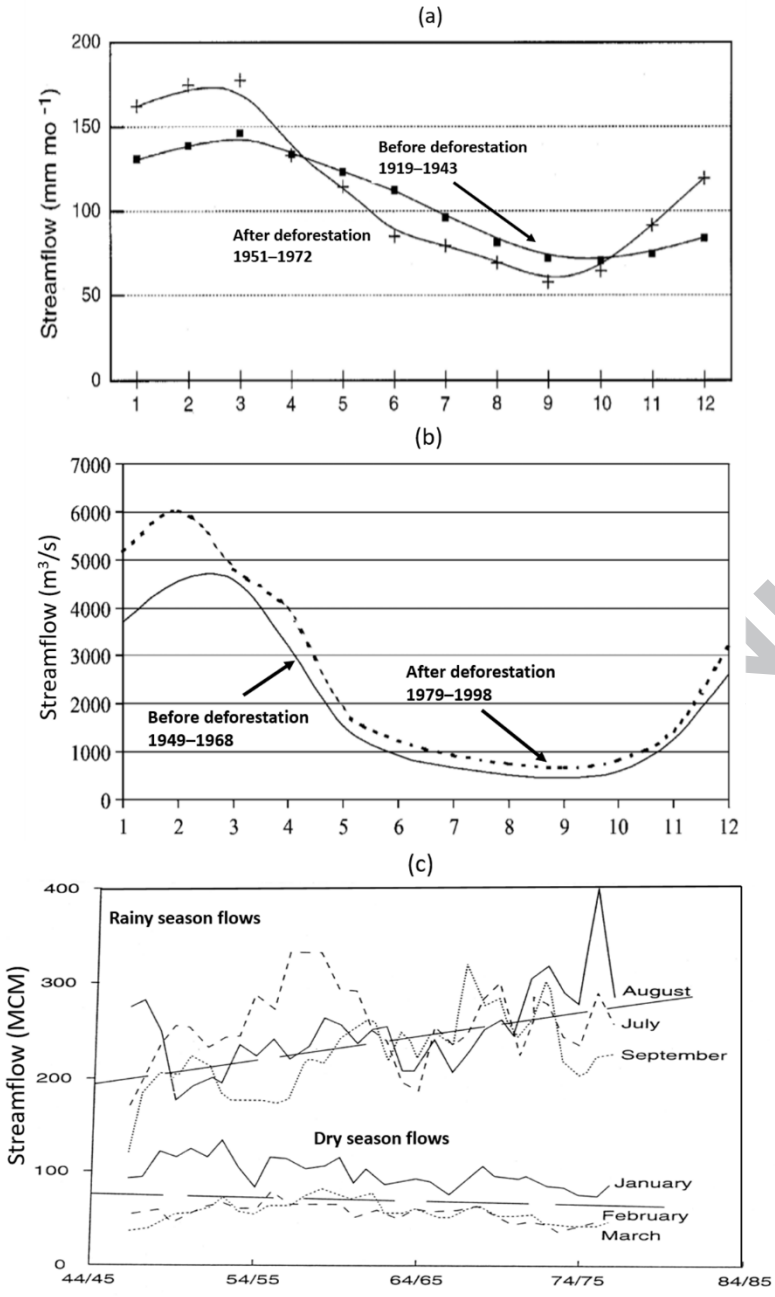

Figure 2. (a) Change in seasonal distribution of streamflow following changes in land use: replacing 33% of forest by rain-fed cropping and settlements in the Upper Konto catchment, East Java, Indonesia (after Rijsdijk and Bruijnzeel, 1991); (b) Idem for the Tocantins catchment, Brazil, where about 19% forest was replaced by cropland and grassland (after Costa et al., 2003); (c) Changes in long-term rainy- and dry-season flows in the Upper Mahaweli catchment, Sri Lanka, where well-managed tea estates were replaced by smallholder cropping without adequate soil conservation measures.

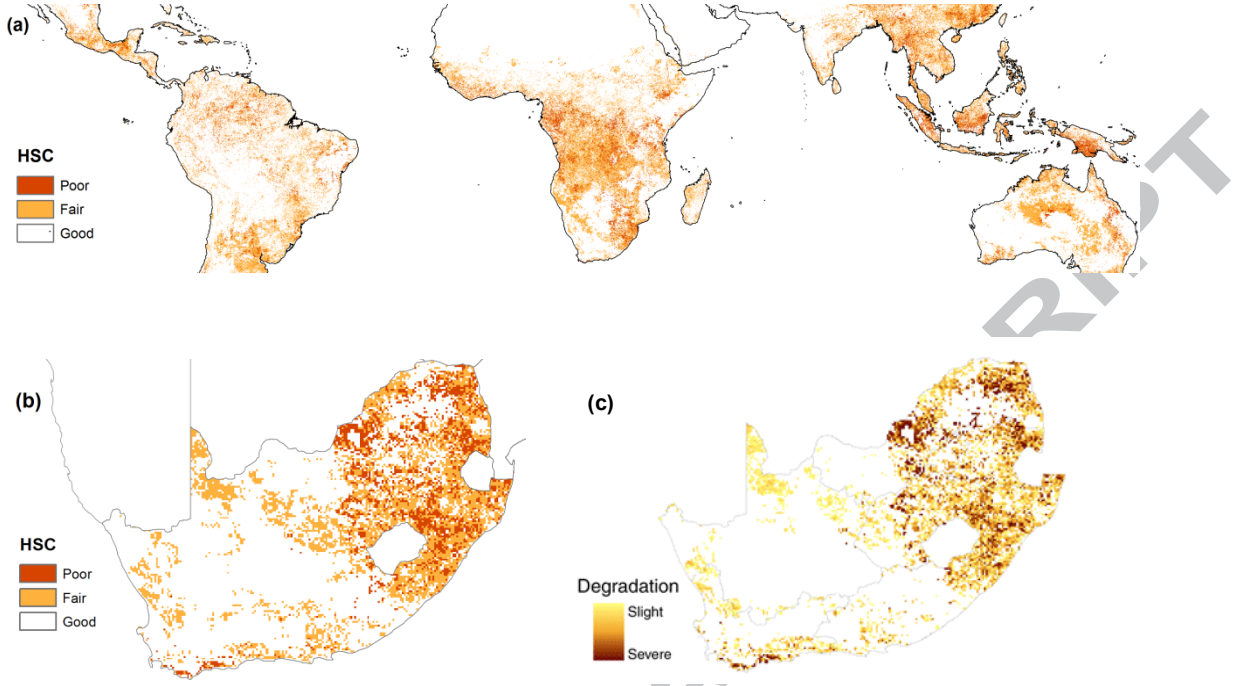

Figure 3. (a) Classification of 'Hydrological Soil Condition' (HSC) based on trends of rainfall use efficiency (RUE)-adjusted normalised NDVI (Bai et al. (2008), see text for explanation); (b) Comparison of HSCs derived in this way for the Republic of South Africa with (c) Land degradation categories as defined in Bai et al. (2008) for RSA. Note that Swaziland, Lesotho and bordering countries are masked in the latter two maps.

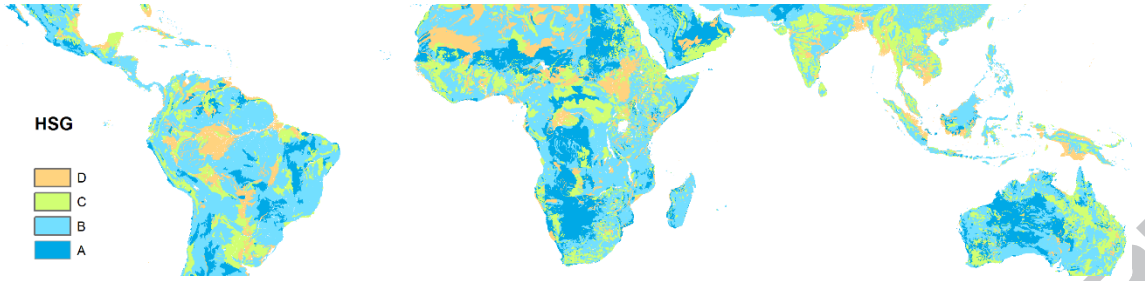

Figure 4. Map of 'Hydrological Soil Groups' (HSG) across the tropics based on the Harmonised World Soil Database (FAO/IIASA/ISRIC/ISSCAS/JRC, 2012).

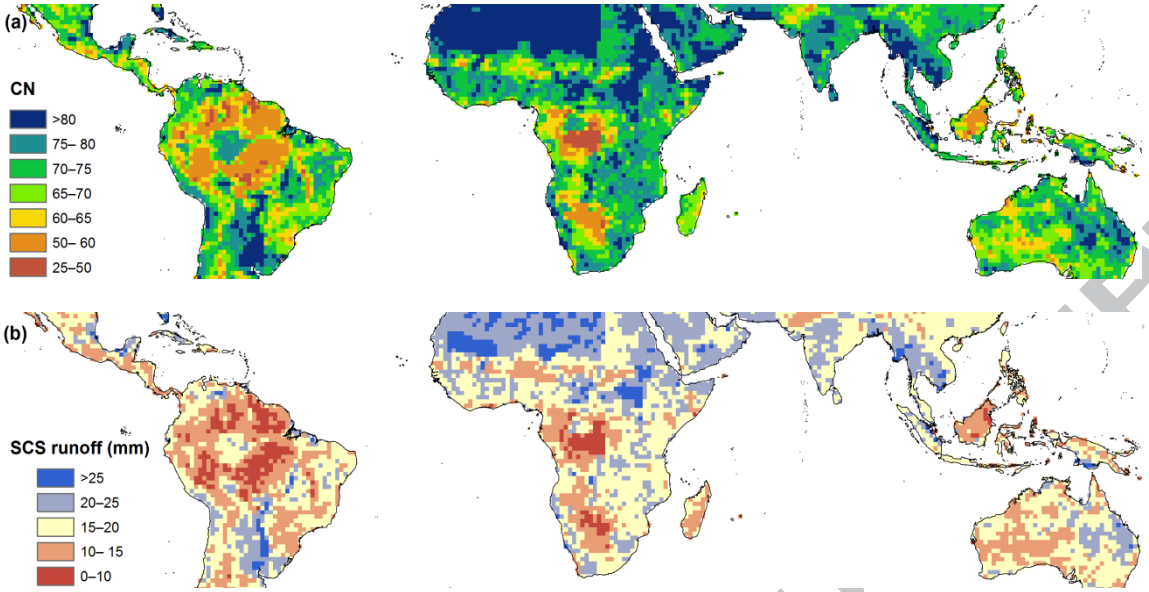

Figure 5. (a) Curve number values (CN) for current land-cover conditions across the tropics; and (b) Associated predicted amounts of stormflow (mm) for a uniformly distributed design rainfall event of 50 mm.

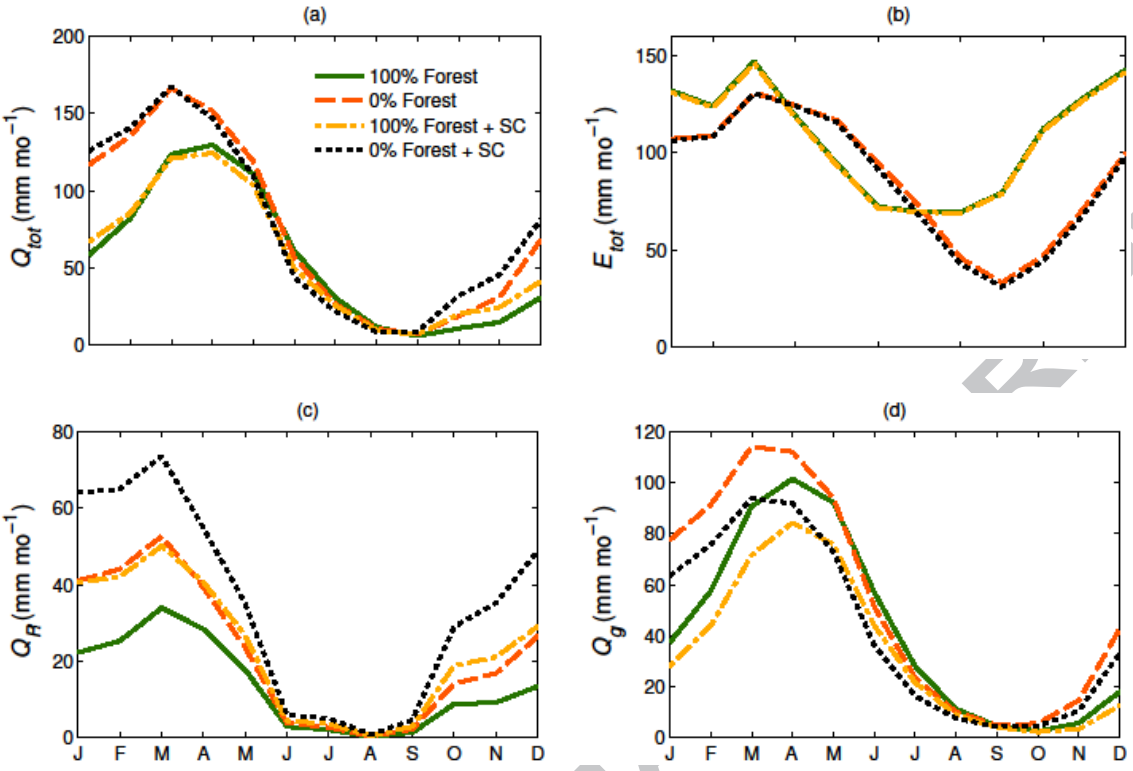

Figure 6. Mean monthly simulated (a) streamflow (Q_{tot}), (b) evapotranspiration (E_{tot}), (c) storm runoff (Q_R) and (d) baseflow (Q_g) for 1948–2008 for the upper Konto catchment, Indonesia. Each coloured line represents simulations depicting different vegetation and surface conditions; the term SC in the legend refers to a negative change in surface infiltration capacity: 100% Forest (100FC, green solid line), 0% Forest (0FC, orange dashed line), 100% Forest +SC (100FCSC, yellow line) and 0% Forest + SC (0FCSC, black dotted line).

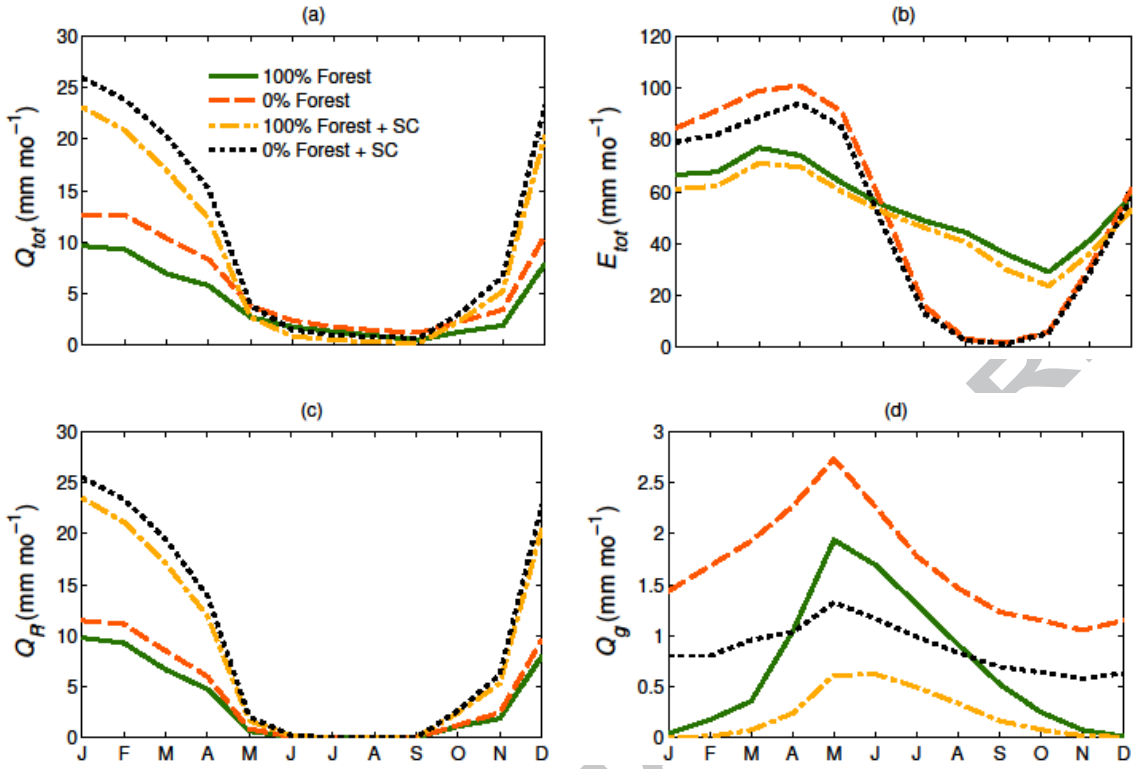

Figure 7. Mean monthly simulated (a) streamflow (Q_{tot}), (b) evapotranspiration (E_{tot}), (c) storm runoff (Q_R) and (d) baseflow (Q_g) for 1948–2008 for the Babati catchment, Tanzania. Each coloured line represents simulations depicting different vegetation and surface conditions; the term SC in the legend refers to a negative change in surface infiltration capacity: 100% Forest (100FC, green solid line), 0% Forest (0FC, orange dashed line), 100% Forest +SC (100FCSC, yellow line) and 0% Forest + SC (0FCSC, black dotted line).

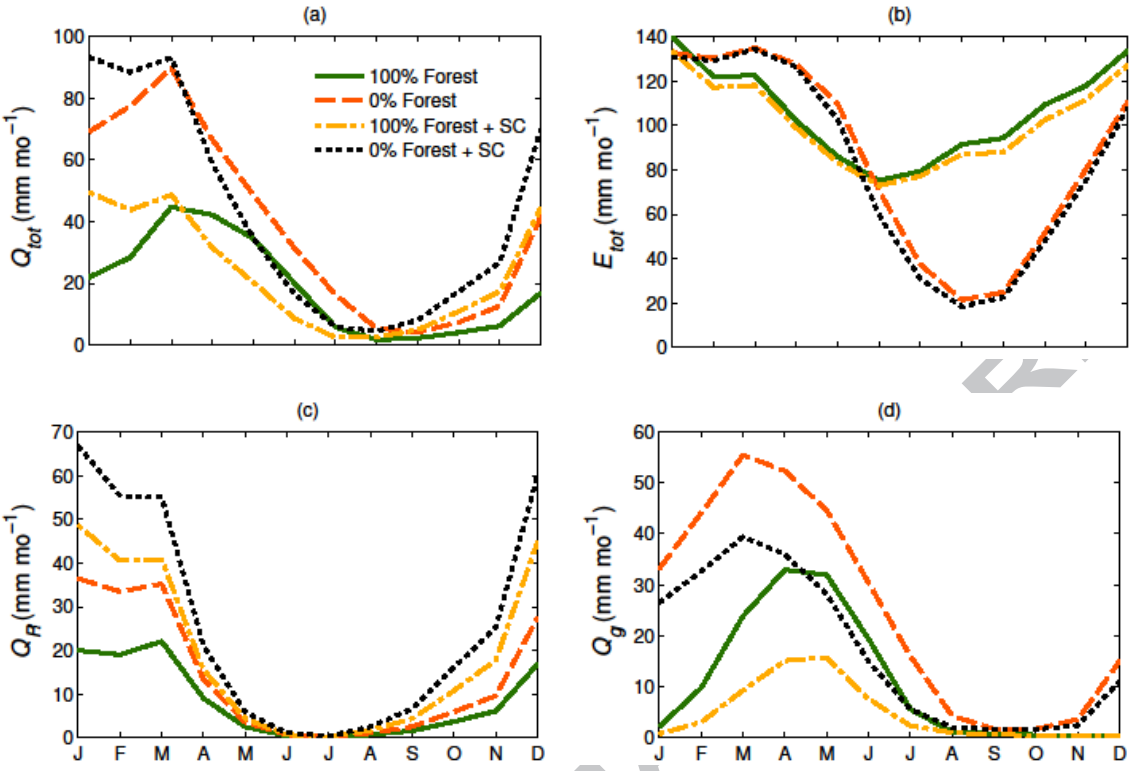

Figure 8. Mean monthly simulated (a) streamflow (Q_{tot}), (b) evapotranspiration (E_{tot}), (c) storm runoff (Q_R) and (d) baseflow (Q_g) for 1948–2008 for the Tocantins catchment, Brazil. Each coloured line represents simulations depicting different vegetation and surface conditions; the term SC in the legend refers to a negative change in surface infiltration capacity: 100% Forest (100FC, green solid line), 0% Forest (0FC, orange dashed line), 100% Forest +SC (100FCSC, yellow line) and 0% Forest + SC (0FCSC, black dotted line).

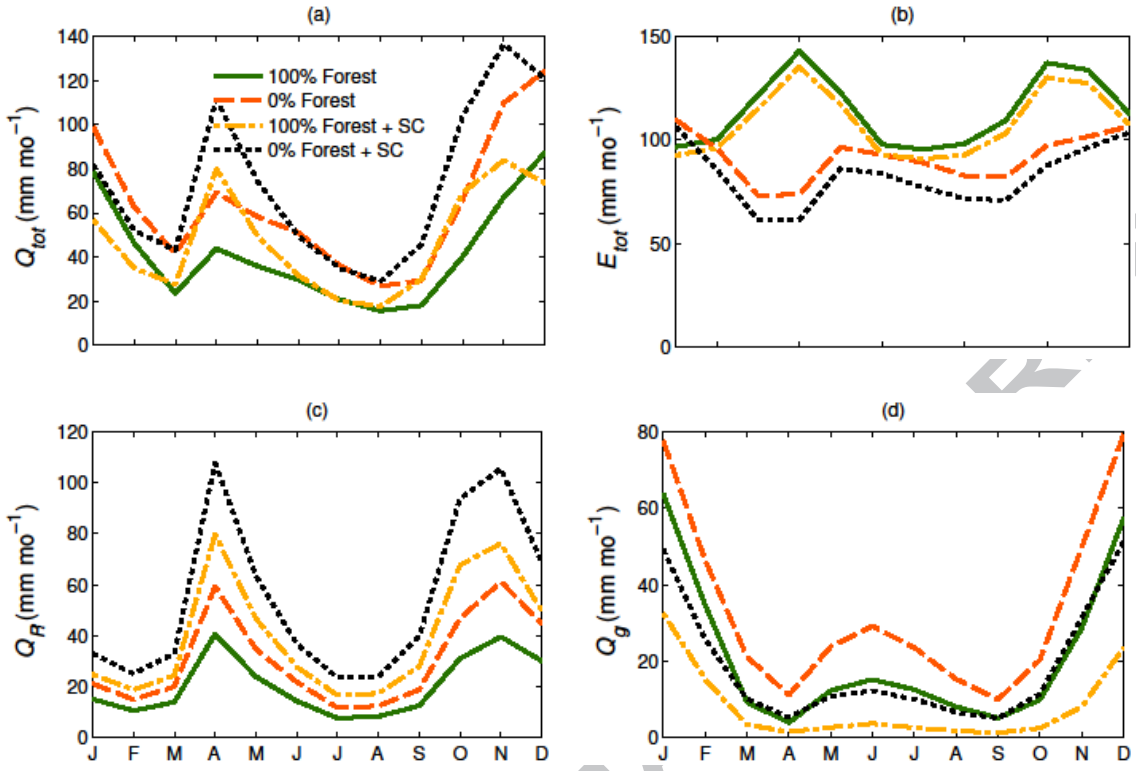

Figure 9. Mean monthly simulated (a) streamflow (Q_{tot}), (b) evapotranspiration (E_{tot}), (c) storm runoff (Q_R) and (d) baseflow (Q_g) for 1948–2008 for the Mahaweli catchment, Sri Lanka. Each coloured line represents simulations depicting different vegetation and surface conditions; the term SC in the legend refers to a negative change in surface infiltration capacity: 100% Forest (100FC, green solid line), 0% Forest (0FC, orange dashed line), 100% Forest +SC (100FCSC, yellow line) and 0% Forest + SC (0FCSC, black dotted line).

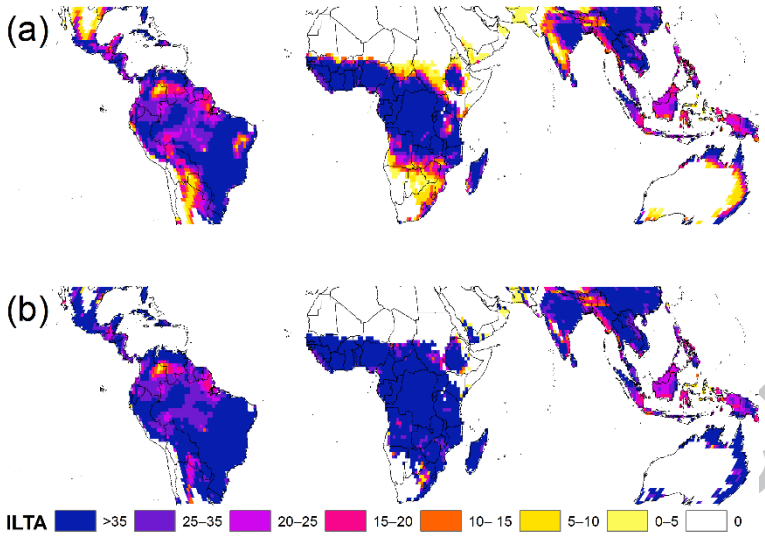

Figure 10. Relative change in long-term mean annual streamflow (ILTA) under deforestation impact and undisturbed conditions, expressed as a percentage of the long-term mean annual streamflow under undisturbed conditions for (a) deforestation only (100FC-0FC); and (b) deforestation plus a negative change in surface infiltration (100FC-0FCSC).

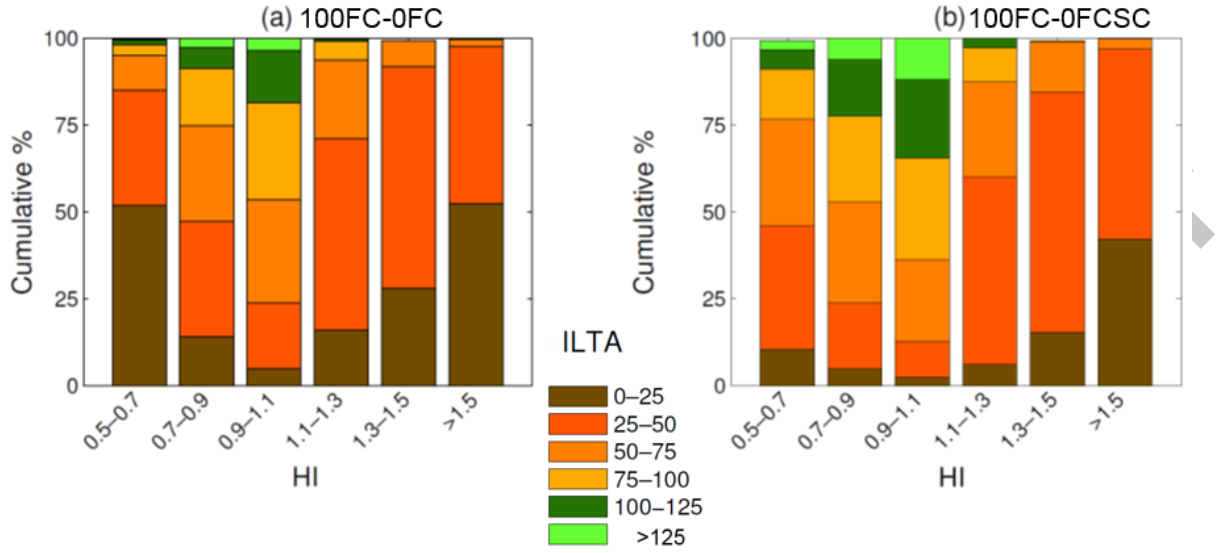

Figure 11. Cumulative percentage relative change in long-term mean annual streamflow (ILTA) grouped by humidity index (HI) for (a) Forest conversion to grassland only (100FC-0FC); and (b) Forest conversion plus surface degradation (100FC-0FCSC). Different ranges in the percentage increase in ILTA are indicated by different colours.

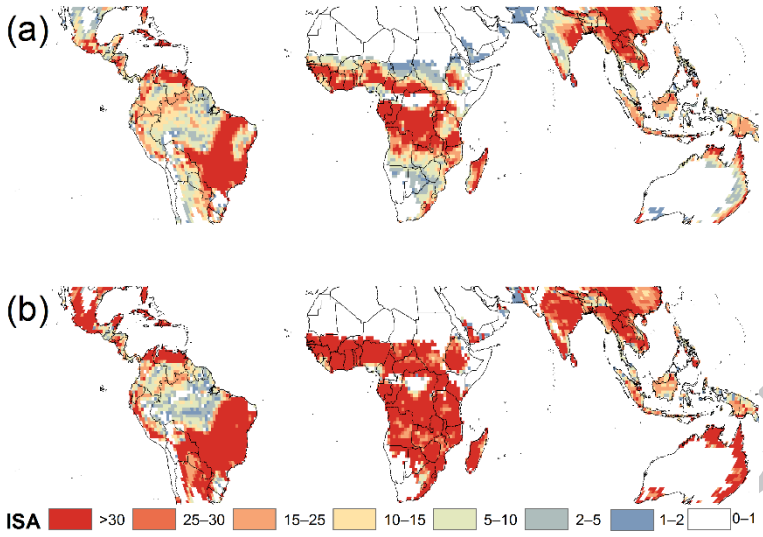

Figure 12. Difference between long-term mean seasonal amplitude (ISA) of streamflow under deforestation impacts and prior conditions, expressed as a percentage of the amplitude under prior conditions for (a) Forest conversion to grassland (100FC-0FC); and (b) Forest conversion plus surface degradation (100FC-0FCSC). See text for explanation.

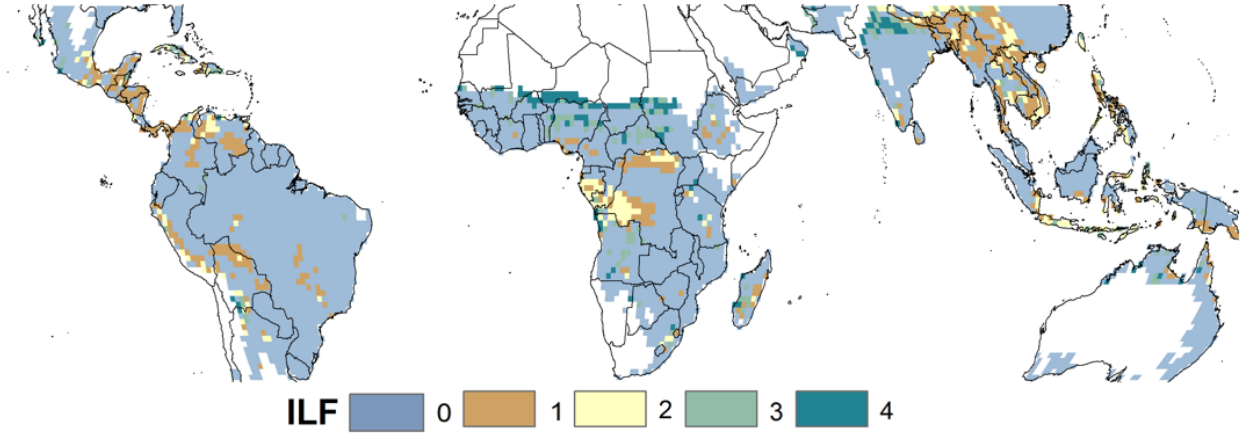

Figure 13. Number of months with simulated decreases in dry-season flows (ILF) out of four months with low flows following forest conversion to grassland and an imposed negative change in soil infiltration capacity (100FC–0FCSC). See text for explanation.

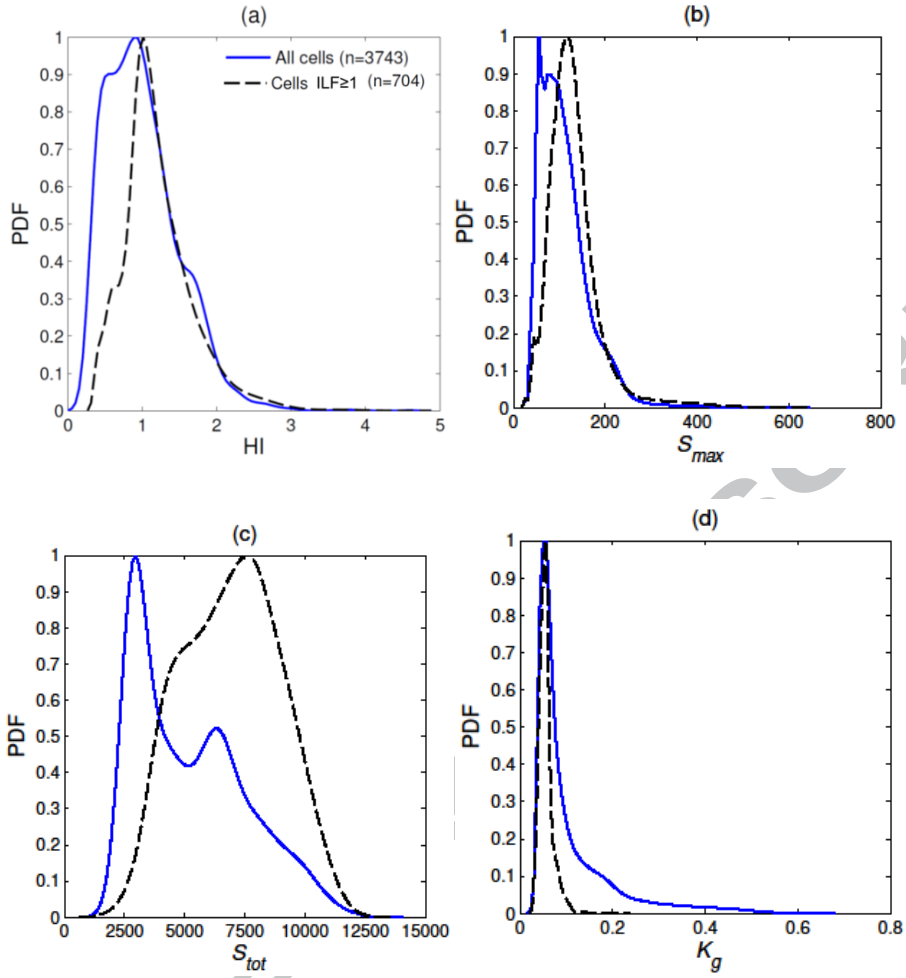

Figure 14. Normalised probability distribution functions (PDF) of all model grid cells (solid blue lines) and of all model grid cells with ILF≥1 (dashed black lines) for mean annual values (1948–2008) of (a) humidity index (HI), (b) potential maximum soil water storage capacity (S_{max}), (c) soil water content in the shallow and deep soil compartments (S_{tot}), and (d) groundwater recession coefficient (K_g).

Table 1. Matching the FAO/UNESCO soil drainage classes with the USDA-SCS Hydrological Soil Groups (HSG).

FAO Drainage class		HSG	
1	Very Poor	D	Very low infiltration rates
2	Poor	D	
3	Imperfectly	C	Low infiltration rates
4	Moderately Well	B	Moderate infiltration rates
5	Well	A	High infiltration rates
6	Somewhat Excessive	A	
7	Excessive	A	

Table 2. Curve numbers (CN) for different land uses and land covers and Hydrological Soil Groups (HSGs) for 'fair', 'poor' and 'good' soil hydrological conditions (HSCs) (modified after USDA-SCS (1986) and Hong and Adler (2008)).

Land use/land cover	Hydrological Soil Group (HSG)											
	Fair HSC*				Poor HSC*				Good HSC*			
	A	B	C	D	A	B	C	D	A	B	C	D
Water bodies	N/A	N/A	N/A	N/A	N/A	N/A	N/A	N/A	N/A	N/A	N/A	N/A
Evergreen needle leaf	36	60	73	79	45	66	77	83	30	55	70	77
Evergreen broad-leaf	30	58	71	77	39	64	75	81	24	53	68	75
Deciduous needle leaf	40	64	77	83	49	70	81	87	34	59	74	81
Deciduous broad-leaf	42	66	79	85	51	72	83	89	36	61	76	83
Mixed forests	38	62	75	81	68	79	86	89	49	69	79	84
Woodlands	61	71	81	89	91	88	92	97	72	78	85	92
Wooded grasslands	55	70	80	87	80	84	89	93	56	70	80	86
Closed shrublands	45	65	75	80	64	75	82	85	35	57	70	76
Open shrublands	49	69	79	84	68	79	86	89	39	61	74	80
Grasslands	49	69	79	84	68	79	86	89	39	61	74	80
Croplands	67	78	85	89	72	81	88	91	61	70	77	80
Bare ground	72	82	83	87	72	82	83	87	72	82	83	87
Urban and built-up	80	85	90	95	80	85	90	95	80	85	90	95

* Hydrological condition indicates the effects of cover type and treatment on infiltration and storm runoff.

Table 3. Location of catchments used in the streamflow sensitivity analyses and associated characteristics including: size, land-use change, mean annual precipitation (MAP), mean annual potential evapotranspiration (PET) and precipitation seasonality index (SI) for the years 1948–2008. Climatic characteristics were computed from the Princeton climate dataset (Sheffield et al., 2006).

Location	Area (km^2)	Land-use change	Effect on dry-season flow	Latitude	Longitude	MAP ($mm\ y^{-1}$)	PET ($mm\ y^{-1}$)	SI*	Main reference
Upper Konto (Indonesia)	235	A third of the area converted to rain-fed cropping	Reduction	7.52°S	112.24°E	1964	1526	0.65	Rijsdijk and Bruijnzeel (1991)
Babati (Tanzania)	2.8	Miombo woodland converted to cropping and grazing	Reduction	4.15 °S	35.46°E	712	2075	0.87	Sandström (1995)
Tocantins (Brazil)	175,360	About 19% converted to grazing	No reduction, but redistribution of seasonal flows	11.05°S	48.25°W	1503	1911	0.82	Costa et al. (2003)
Upper Mahaweli (Sri Lanka)	1100	Well-managed tea estates converted to smallholder cropping without soil conservation measures	Reduction	7.12 °N	80.40°E	1878	2033	0.37	Madduma Bandara (1997)

* SI (Walsh and Lawler, 1981) indicates the intra-annual seasonality of precipitation. It varies from zero (all months with the same precipitation) to 1.83 (all precipitation occurring in one month): values <0.19 indicate very equal precipitation, whereas values between 0.20 and 0.99 indicate a seasonal regime and values >1 a short wet season.

Table 4. Comparison of climatic and physical characteristics of all model grid cells with those of cells with a decrease in dry-season flow for at least one month (ILF≥1). Climatic characteristics include means and standard deviations (in brackets) of: mean annual precipitation (MAP), humidity index (HI) and seasonality index (SI). Physical characteristics include: potential maximum soil water storage capacity for rainfall events (S_{max}), soil water content in the shallow and deep soil compartments (S_{tot}), and the groundwater recession constant (K_g).

Characteristic	All grid cells (n = 3743)	Grid cells ILF≥1 (n = 704)
Climatic		
MAP (mm y^{-1})	1513 (±652)	1690 (±747)
HI	0.70 (±0.58)	1.20 (±0.47)
SI	0.63 (±0.28)	0.62 (±0.19)
Physical		
S_{max}	112 (±62)	135 (±76)
$S_{tot} = S_s + S_d S_0$ (mm)	5449 (±4586)	7531 (±3742)
S_{totFC} (mm)	832 (±367)	1200 (±370)
K_g (day^{-1})	0.11 (±0.09)	0.06 (±0.01)

Research highlights

- Evaluation of the impacts of deforestation on the water balance across the tropics (84 characters including spaces)
- Three relevant indicators of streamflow regime change computed across the tropics (83 characters including spaces)
- Exploration of biophysical and climatic controls for reductions in dry season flows (85 characters including spaces)
- 'Hot spots' of post-deforestation negative impacts (reduction) on dry season flows (84 characters including spaces)
- 'Hot spots' found in all continents in the tropic in areas with seasonal regimes (82 characters including spaces)